OCULUS ATTITUDE CONTROL SYSTEM

By

MARY FARMER

A THESIS

Submitted in partial fulfillment of the requirements

for the degree of

MASTER OF SCIENCE IN MECHANICAL ENGINEERING

MICHIGAN TECHNOLOGICAL UNIVERSITY

2008

This thesis, "Oculus Attitude Control System", is hereby approved in partial fulfillment of the requirements for the degree of MASTER OF SCIENCE in Mechanical Engineering.

DEPARTMENT:
Mechanical Engineering - Engineering Mechanics

Signatures:

Thesis Advisor ____

Dr. Gordon G. Parker

Co-Advisor ____

Dr. Lyon B. King

Department Chair ____

Dr. William W. Predebon

Date ____

Dedication

To my dogs, Cleo and Vinnie, who are sitting behind me chewing on each other as I type this.

Abstract

The Oculus is a nanosatellite being developed at Michigan Technological University as an entry into the Air Force Research Laboratory's University Nanosat 5 competition. The mission chosen for the Oculus is to demonstrate technologies needed to create a low-cost space situational awareness satellite on a nanosatellite platform. This thesis presents the attitude determination and control system needed to complete the space situational awareness technology demonstration mission.

In the beginning of this thesis, the operating modes of the Oculus are discussed in relation to the mission and available hardware. The hardware available on the Oculus includes three reaction wheels, three magnetic torque rods, a three-axis gyroscope and a three-axis magnetometer. Before the controllers are presented, a description of the dynamics and kinematics of the satellite is given. The two main controllers on the Oculus are presented following the dynamics and kinematics description. The reaction wheel controller is mainly used for the visual servoing task when precise attitude control is necessary. The magnetic torque rod controller is used for general orientation of the satellite and momentum management. Finally, the attitude estimator, using the magnetometer and gyroscopes, is presented. Dynamic simulation results are presented for both the controllers and attitude estimators in their respective chapters.

Acknowledgments

I would like thank my advisors, Dr. Gordon Parker and Dr. Lyon B. King for all their support and guidance while I was working on the Oculus. Numerous times they have helped to point me in the correct direction.

I would like to thank all of the Oculus team members that I've worked with on this program. Without them, the Oculus would have never been proposed or made it as far as it has.

I would also like to thank the Air Force Research Laboratory for organizing and sponsoring the Nanosat-5 competition. Without this competition, The Oculus would not exist.

Finally, I'd like to thank my family, foremost my husband Brian McPherson for putting up with me while I've worked on the Oculus project and this thesis and my parents, David and Marilyn Farmer for so many numerous things I can't begin to express all of them here.

Contents

List of Figures

List of Tables

Chapter 1

Introduction

The Oculus is a satellite being designed and fabricated by students at Michigan Technological University. The Oculus is an entry into the Air Force Research Laboratory's (AFRL) fifth University Nanosatellite (Nanosat-5) Competition. Each competing team selects their own mission; the mission chosen by the Michigan Tech team is to develop and demonstrate a nanosatellite platform capable of acquiring, imaging, tracking, and monitoring objects within the local vicinity (1 km) of the vehicle. This mission will provide a test bed for the technologies needed for space-based space situational awareness (SSA).

The Nanosat competition is held at two year intervals and at the beginning of each two year competition cycle, universities prepare and submit satellite proposals from which ten to twelve universities are selected to compete. Once selected to compete, the universities have two years to design and fabricate a satellite. At the completion of these two years, one satellite is chosen for launch and the University continues to work closely with AFRL to prepare the satellite for launch.

As part of the proposal, the mission for the Oculus, space based SSA, was selected. Space situational awareness is best defined by Lt. Col. Shoemaker, the Program Manager of the Tactical Technology Office at DARPA Space Activities, as "means knowing the location of every object orbiting the Earth, active or inactive, big or small; and knowing why it is there, what it is doing now, and what we think it will be doing in the future."[16] The Oculus is a testbed for the technologies needed to to create a fleet of small SSA satellites that could be used to build a satellite network to monitor objects in Earth's orbit. A three-axis attitude determination and control system is required to complete the Oculus' SSA mission.

Historically, many larger satellites have utilized three-axis attitude determination and control systems. More recently these system have begun to be implemented on smaller platforms. The Oculus is on the leading edge of miniaturizing satellite three-axis attitude determination and control.

1.1 Aim and Scope

The aim of this thesis is to establish the attitude determination and control system algorithms that are the building blocks for completing the SSA mission of the Oculus.

Two main constraints exist which dictate the design for the Oculus, the performance requirements needed to fulfill the SSA mission and the hardware available on the Oculus. The performance requirements are a derivative of the system requirements for the Oculus. Determining the performance requirements are outside the scope of this thesis. The requirements of the Oculus attitude determination and control system are as follows:

1. The attitude control system shall be capable of detumbling from an absolute angular velocity of 6 degrees/sec/axis to less than 1 degree/sec/axis on all 3 axes with a goal time of less than one hour.

2. The attitude control system shall be capable of slewing at a rate of 30 deg/sec for high speed pointing accuracy.

3. The attitude control system shall be capable of maintaining attitude with 0.15 deg pointing accuracy while tracking or monitoring.

4. The attitude control system shall track objects detected by the imaging apparatus.

5. The attitude control system shall have enough momentum storage capacity to counter external torques and make pointing adjustments for one orbit.

6. The attitude control system shall be capable of orienting the satellite for maximum power generation from solar cells while not tracking or monitoring.

These requirements are all used to develop the Oculus attitude determination and control algorithms except requirement 5, which is a hardware requirement.

Selection of the hardware available for the attitude determination and control system was outside the scope of the this thesis and was selected before the development of the algorithms began. Size, cost, and availability dictated the attitude determination and control hardware the Oculus is equipped with. The Oculus attitude determination and control system is designed to utilize the hardware the Oculus is equipped with to create a system capable of in-space SSA.

The scope of this thesis is limited to the attitude determination and control algorithms utilizing the hardware selected for the Oculus. The three algorithms developed are the reaction wheel controller, the magnetic torque rod controller, and the attitude estimator.

While this work was motivated by the needs of the Oculus mission requirements, a contribution to the general topic of spacecraft attitude determination and control was made. Specifically, the new work in this thesis includes the magnetic torque rod controller and the extended Kalman filter attitude estimator. The magnetic torque rod controller extends the use of modified Rodrigues parameters to attitude control using only the magnetic torque rods for actuation. The modified Rodrigues parameters are a more elegent, three parameter, representation of attitude compared to Euler parameters which are a four parameter representation. The extended Kalman filter attitude estimator, discussed in the sixth chapter, uses single vector measurements along with rate measurements to estimate the attitude of the satellite. The unique part of this estimator is the use of Baumgarte constraint stabilization to dynamically maintain the constraint on Euler parameters which is discussed in the third chapter.

1.2 Overview

Following this chapter, the groundwork required for developing the attitude determination and control algorithms is presented. The second chapter of this thesis presents the configuration of the Oculus with respect to its attitude determination and control hardware. Each sensor and actuator is described along with how they work together to accomplish the Oculus mission. Also, in the second chapter the mission evolution of the Oculus is presented where the different stages of the Oculus mission are described from with detumbling after launch to visual referenced object tracking. The third chapter of this thesis presents the dynamics and kinematics of the Oculus. These dynamics and kinematics are used for both developing and simulating the algorithms in the three chapters that follow.

Chapter 4 and Chapter 5 present the two controllers, first the reaction wheel controller and second the magnetic torque rod controller, used on the Oculus. These control algorithms utilize the Oculus dynamics developed in Chapter 3 in the analysis of the controller and utilize both the dynamics and kinematics in the simulation of the control algorithm.

Chapter 6 deals with the attitude determination part of the attitude determination and control system. In this chapter the dynamics and kinematics are used to develop a Kalman filter attitude estimator. Simulation results are presented for this attitude estimator.

Finally, in Chapter 7 conclusions are drawn which relate the algorithms developed with the requirements for the attitude determination and control system.

Chapter 2

Attitude Determination and Control Configuration

In this chapter, the Oculus' attitude control components are described in relationship to the satellite's modes of operation. First, an overview of the Oculus mission is given, emphasizing its mode-dependent attitude control objectives. This is followed by a description of the specific sensors and actuators selected. Finally, a description of how the attitude control components are used to satisfy the attitude control objectives is given.

The Oculus will be separated from its launch vehicle with an expected 6 degrees/second rotation in all three body axes. The first objective of the attitude control system is to detumble the spacecraft. After stabilizing the spacecraft and establishing ground station communication, the Oculus will attempt to track self-deployed cubesats. The final objective is to test its tracking capability on a known target such as the International Space Station (ISS).

2.1 Sensors

The Oculus sensor suite consists of a three-axis gyroscope, a three-axis magnetometer, a vision system, and a clock. The gyroscope and magnetometer, shown in Figure 2.1, are used for inertially referenced attitude estimation and closed loop attitude control, exclusive of target tracking. The vision system consists of two cameras. The wide field of view (WFOV) camera is used to identify the general location of a target. The narrow field of view (NFOV), low-light camera is used in conjunction with closed loop visual servoing to track the identified targets.

2.2 Actuators

The spacecraft has both a magnetic torque rod system and a reaction wheel system for applying control moments to the satellite. The magnetic torque rods are used for both detumble and non-tracking attitude control along with desaturating the reaction

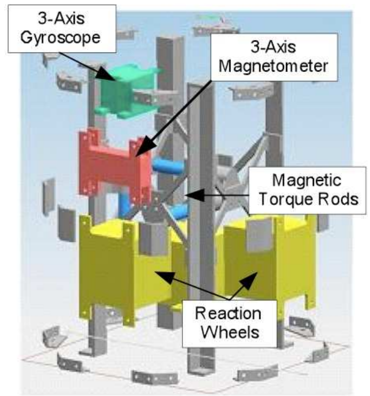

Figure 2.1: Oculus configuration with respect to the attitude sensors and actuators.

wheels. The reaction wheels, shown in Figure 2.1, are used for attitude control during visual tracking operations due to their higher level of precision control.

2.3 Mission Evolution

The Oculus attitude control hardware was selected based on its ability to accomplish and fit within the mission goals, budget, and available space. A diagram of the attitude control system is shown in Figure 2.2. Initial detumbling of the satellite will rely on the magnetic torque rods. The control system will read in magnetometer data and use this to generate the desired currents in the rods that will result in torques generated by the torque rods to drive the satellite rotational velocity to zero.

The Oculus satellite will have an onboard orbital model of its current position using

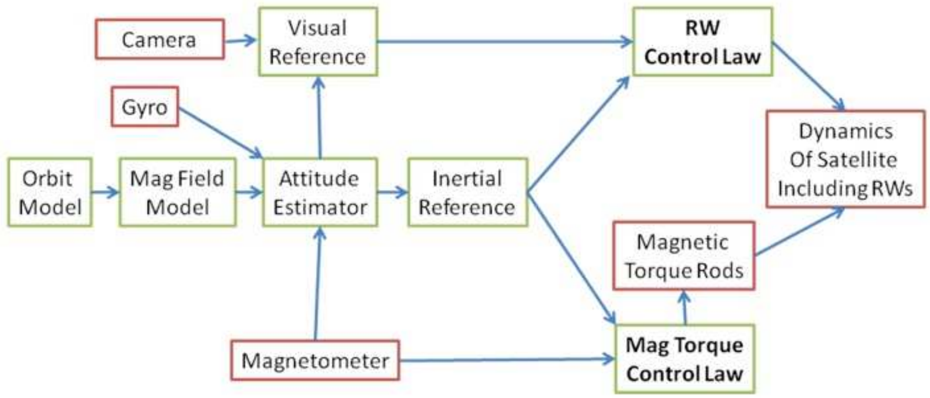

Figure 2.2: Overview of the Oculus attitude determination and control system showing the interaction between elements.

the Simplified General Perturbations Satellite Orbit Model 4 (SGP4) algorithm. This position is used to calculate a modeled magnetic field vector using the world magnetic model (WMM). A Kalman filter attitude estimator will couple these two models, along with the magnetometer and gyroscope reading, to inertially reference the attitude.

The first mission objective will be to orient the satellite's antennas for ground communication. This maneuver will be conducted multiple times throughout mission lifetime for uploading commands to the satellite and downloading stored images.

The SSA objectives will all follow a similar control path. First, the satellite will use the reaction wheels to point its imagers at an expected target and start capturing images. The images will be analyzed autonomously by onboard image recognition and tracking software. Once an object is identified, the 3-axis control system will transition from being inertially referenced, where the attitude error of the satellite is described relative to a fixed frame, to being visually referenced, where the attitude error of the satellite is described relative to an object being viewed by the imager. This handoff will change what is producing the attitude control error but will not change the control laws which govern the reaction wheels. Throughout the visual tracking operation, the control system will continually save images to disk while keeping the object centered in the camera's field of view.

External disturbance torques will be detected as a standard attitude error by the control system and automatically mitigated[21]. The magnetic torque rods will be used to desaturate the reaction wheels during non-manuevering operational times when reaction wheels have unnecessary momentum.

Chapter 3

Literature Review

In this chapter, a literature review of the main components of the attitude determination and control systems are presented.

Creating an attitude determination and control system for a nanosatellite such as the Oculus includes a broad range of topics. The purpose of this thesis is to present the basic building blocks needed for a successful attitude determination and control system. The hardware chosen for the Oculus dictated the starting point for the attitude determination and control system. These basic building blocks are the reaction wheel controller, magnetic torque rod controller, and attitude estimator. This chapter will first discuss existing work related to the reaction wheel controller. The magnetic torque rod controller will be discussed second. Finally, the attitude estimator is discussed.

Because of the broad range of topics covered in this thesis, this literature review is not intended to give an exhaustive coverage of all topics related to the Oculus attitude determination and control system but instead present a sampling of available work related to the main components of the system.

3.1 Reaction Wheel Control

The Oculus attitude control system starts with the reaction wheel controller. Reaction wheels have been common control actuators used on satellites from the beginning of the space race. In 1959, reaction wheels were introduced for use as control actuators for satellites as described by Papapoff and Froelich [5]. The authors present an example of reaction wheel control where a single axis experiment was constructed to demonstrate their feasibility.

Many different approaches have been taken to the reaction wheel control problem since their introduction in 1959. A number of practical issues relating to reaction wheel control have been addressed throughout the years. One issue that could be faced in any attitude control system is a lack of rate measurement. Nicosia and Tomei[8] propose an attitude controller using only angular position measurements. To gain the rate information necessary for the model dependent control, a state observer was developed. An observer such as this is not necessary for the Oculus because rate information is available from the gyroscopes.

A number of reaction wheel controllers have been developed to deal with parametric and nonparametric uncertainty in the satellite and reaction wheel dynamics and disturbance torques. A model reference adaptive control law was developed by Singh [17] to deal with these uncertainties. Sadati et al.[14] developed a neural network approach to the reaction wheel control problem which allowed for uncertainty in mass properities. Milti-input multi-output (MIMO) quantative feedback theory (QFT) approach is used by Nudehi et al. [9] which again had the ability to satisfy performance objectives amongst uncertain system parameters. Finally, Robinett and Parker [10] discussed the use of sliding mode control for reaction wheel control of spacecraft to create a system robust to initial condition and mass property uncertainty.

Simplicity is one of the top priorities for all of Oculus' systems. It is believed that the system parameters of the Oculus will be well characterized and there will be minimal disturbance torques on the satellite. As a result, a controller more simple than those discussed above is preferable. The controller used on the Oculus is developed by Schaub and Junkins[15] and is discussed in detail in Chapter 5 of this thesis. The unique part of this controller is the use of Modified Rodrigues Parameters (MRP) to represent the orientation of the satellite. All the reaction wheel control strategies above used either Euler parameters or Euler angles. The MRPs used for reaction wheel control are also used in the magnetic torque rod control strategy described below.

3.2 Magnetic Torque Rod Control

Magnetic torque rods are another popular attitude control device for satellites. The main purpose of the magnetic torque rods on the Oculus are to provide pure torques allowing for the desaturation of the reaction wheels which can store unwanted momentum as a result of launch and disturbance torques. The Oculus is able to transfer momentum from the reaction wheels to the satellite using reaction wheel speed control. This results in general three-axis rotation of the satellite. The magnetic torque rod controller must be capable of stabilizing the satellite by driving the absolute angular velocity of the satellite to zero. Secondary to their use to desaturate the reaction wheels, they will also be used to orient the satellite for communication with the ground stations. For this application, only rough pointing accuracy is necessary to prevent the satellite from orienting the communication antennas' blind cones directly toward the ground station.

A number of different approaches have been taken to tackle the magnetic torque rod control problem. D'Andrea and Psiaki[13] proposed three different approaches to the attitude control application. Simulation results from these were presented and performance was compared. The three approaches were (1) linear quadratic regulator (LQR), (2) sliding mode-like control, and (3) H_∞. All three of these controllers were able to accomplish the attitude control task required on the Oculus and each have their advantages. Another H_∞ controller was developed by Kulkarni and Campbell[7] which built on the work by D'Andrea and Psiaki[13]. Like the controllers developed by D'Andrea and Psiaki [13], this controller was shown to be robust to uncertainty in the magnetic field as a result of modeling error. In a continuation of the work completed by D'Andrea and Psiaki[13], the LQR controller was considered in greater depth by Psiaki[12].

Astolfi and Lovera[1] presented two magnetic torque rod controllers, one of which is the basis for the magnetic torque rod controller used on the Oculus. Since this controller used rate feedback it was of particular interest to the Oculus project because of the body rate measurement which are read from the gyroscopes on the Oculus. Generalized averaging, along with Lyapunov's direct method, was used to demonstrate the stability of this Euler Parameter controller. The controller developed in Chapter 6 for the Oculus is a variation of the same proportional-derivitive form but with MRPs to represent the error in orientation.

3.3 Attitude Estimation

The final component of the Oculus attitude determination and control system is the attitude estimator. Many attitude determination methods use two or more vector measurements to determine the orientation of the satellite as described by Wertz[20]. On the Oculus, only one vector measurement, the magnetic field vector is available. In addition to this vector, the angular velocity, which is read from the gyroscopes, is also available. The attitude of the Oculus can not be directly calculated based on these measurements and thus an attitude estimator is required.

A number of attitude estimators have been developed which determine the orientation of the satellite from gyroscope and magnetometer measurements. Peck[11] used a generic single vector measurement along with body rates from the gyroscope to develop an attitude estimator using a two-step autoregressive filter. This method suggests using infrequent single vector measurements to correct drift and error caused by integration of the body rates measured by the gyroscopes. The benefit of less frequent vector measurements is a reduction in the processing burden, which is attractive for the Oculus application.

You et al.[18] develop an estimator using a micro inertial measurement unit (MIMU), with three gyros and three accelerometers, in addition to a magnetometer. For attitude determination, only the angular velocity measurement is used from the MIMU.

Two different filtering methods, the extended Kalman filter (EKF) and the unscented Kalman(UKF) filter are developed and compared. Both filtering methods are capable of determining the orientation of the satellite but the UKF had better performance than the EKF.

Kalman filters are popular for use as attitude estimators. Traditionally the Kalman filter is not designed to preserve the magnitude constraint of Euler parameters, which is discussed in detail in Chapter 4. Choukroun et al. introduced a new measurement model which avoided the difficulties in preserving the Euler parameter constraint.

The Oculus attitude estimator is presented in Chapter 7. Unlike the controllers on the Oculus which used MRPs to represent the orientation of the satellite, the attitude estimator represents attitude using Euler Parameters. The Euler parameter constraint is preserved using Baumgarte Stabilization[2].

Chapter 4

Oculus Dynamics and Kinematics

In this chapter, the dynamics and kinematics of the Oculus are discussed. The dynamics of the Oculus are developed starting with the angular momentum of the system. Next, the kinematics of the system are described using Euler Parameters. Finally the Euler Parameters are related to another attitude parameterization, Modified Rodrigues Parameters.

4.1 Dynamics

The first step in designing and simulating the reaction wheel control system necessary for visual servoing is to develop the equations of motion for the dynamics of the satellite. The dynamics incorporate both the satellite structure and the reaction wheels. The Oculus has three identical reaction wheels all mounted orthogonally to each other as shown in Figure 4.1. The body coordinate frame is selected so each body axis is aligned with a spin axis of a reaction wheel.

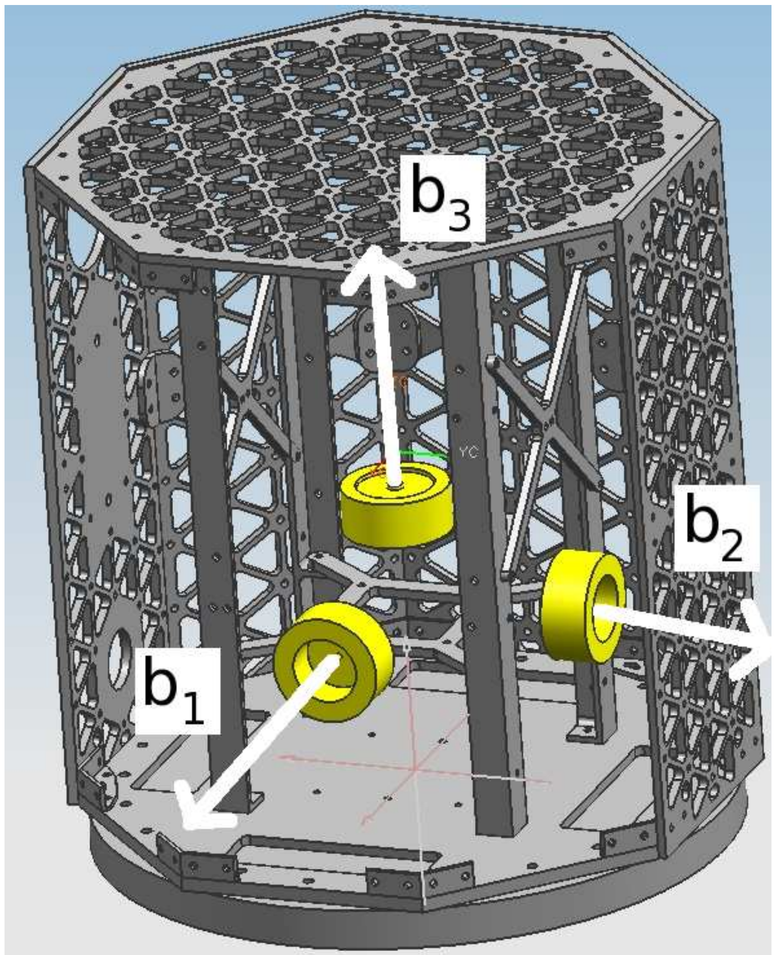

Figure 4.1: Satellite configuration showing reaction wheel placement.

Before moving any further into the satellite dynamics the inertia matrices must be defined. The moment of inertias of the reaction wheels about the spin axis of all three reaction wheels are combined into one inertia matrix, $\mathbf{J}$, shown in Eq. (4.1)

$$\mathbf{J} = \begin{bmatrix} J_{s1} & 0 & 0 \\ 0 & J_{s2} & 0 \\ 0 & 0 & J_{s3} \end{bmatrix}. \tag{4.1}$$

where J_{s1}, J_{s2}, and J_{s3}, are the spin axis inertias of the reaction wheels aligned with the body frame axis. The inertia matrix of the satellite without the inertias of the spin axes of the reaction wheels is defined as $\mathbf{I}$ and is shown in Eq. (4.2)

$$\mathbf{I} = \begin{bmatrix} I_{11} & I_{12} & I_{13} \\ I_{12} & I_{22} & I_{23} \\ I_{13} & I_{23} & I_{33} \end{bmatrix}. \tag{4.2}$$

where it is assumed that $\mathbf{I}$ is constant. It should be noted that $\mathbf{I}$ will need to be updated once the cubesats are deployed.

The analysis of the satellite dynamics begins with the total angular momentum, $\vec{H}$, show in Eq. (4.3)

$$\vec{H} = \mathbf{I}\vec{\omega} + \mathbf{J}(\vec{\omega} + \vec{\Omega}) = (\mathbf{I} + \mathbf{J})\vec{\omega} + \mathbf{J}\vec{\Omega} \tag{4.3}$$

where $\vec{\omega}$ is the absolute angular velocity of the satellite and $\vec{\Omega}$ is the sum of the angular velocities of the reaction wheels relative to the satellite body frame about their spin axes and is given in Eq. (4.4)

$$\vec{\Omega} = \Omega_1 \vec{b}_1 + \Omega_2 \vec{b}_2 + \Omega_3 \vec{b}_3. \tag{4.4}$$

Next, the angular momentum of Eq. (4.3) is differentiated with respect to time to yield the attitude dynamic equations shown in Eq. (4.5)

$$\vec{M} = \dot{\vec{H}} + \omega \times \vec{H} = (\mathbf{I} + \mathbf{J})\dot{\vec{\omega}} + \mathbf{J}\dot{\vec{\Omega}} + \vec{\omega} \times ((\mathbf{I} + \mathbf{J})\vec{\omega} + \mathbf{J}\vec{\Omega}) \tag{4.5}$$

where $\vec{M}$ is a vector of external moments, including magnetic torque rod moments, $\vec{u}$, and disturbance torques, $\vec{w}$. Finally, the relationship between the reaction wheel motor torques, $\vec{T}$, and the angular acceleration is given in Eq. (4.6)

$$\vec{T} = \mathbf{J}(\dot{\vec{\omega}} + \dot{\vec{\Omega}}). \tag{4.6}$$

4.2 Kinematics

The attitude of the satellite can be represented using Euler parameters. Unlike Euler angles which have a singularity that is dependent on the order of rotation, Euler parameters do not have a singularity. Euler parameters describe an object's attitude by defining a unit vector, $\vec{r}$, and a rotation about that vector, Φ, as defined in Eq. (4.7)

$$e_1 = r_1 \sin\frac{\Phi}{2} \quad e_2 = r_2 \sin\frac{\Phi}{2} \quad e_3 = r_3 \sin\frac{\Phi}{2} \quad e_4 = \cos\frac{\Phi}{2} \tag{4.7}$$

where the four Euler parameters are not independent and are related through Eq. (4.8)

$$e_1^2 + e_2^2 + e_3^2 + e_4^2 = 1. \tag{4.8}$$

The Euler parameter representation of attitude related to the angular velocity of the satellite is given in Eq. (4.9)

$$\begin{bmatrix} \omega_1 \\ \omega_2 \\ \omega_3 \end{bmatrix} = 2 \begin{bmatrix} e_4 & e_3 & -e_2 & -e_1 \\ -e_3 & e_4 & e_1 & -e_2 \\ e_2 & -e_1 & e_4 & -e_3 \end{bmatrix} \begin{bmatrix} \dot{e}_1 \\ \dot{e}_2 \\ \dot{e}_3 \\ \dot{e}_4 \end{bmatrix}. \tag{4.9}$$

To ensure that the Euler parameter constraint in Eq. (4.8) is satisfied during simulation and attitude determination, Baumgarte stabilization is used[2]. Baumgarte stabilization allows constraint violations to be dynamically mitigated by replacing the constraint equation with a stable ordinary differential equation (ODE). For the Oculus, the constraint equation is shown in Eq. (4.10)

$$N = e_1^2 + e_2^2 + e_3^2 + e_4^2 - 1 = 0. \tag{4.10}$$

To construct the ODE the constraint is replaced with Eq. (4.11)

$$\dot{N} + cN = 2e_1\dot{e_1} + 2e_2\dot{e_2} + 2e_3\dot{e_3} + 2e_4\dot{e_4} + c(e_1^2 + e_2^2 + e_3^2 + e_4^2 - 1) = 0 \tag{4.11}$$

where c is the pole location of the stabilization dynamics.

The ODE creates a fourth equation which is added to the kinematic equations shown prevously to yield a new set of kinematic equations shown in Eq. (4.12)

$$\begin{bmatrix} \omega_1 \\ \omega_2 \\ \omega_3 \\ -c(e_1^2 + e_2^2 + e_3^2 + e_4^2 - 1) \end{bmatrix} = 2 \begin{bmatrix} e_4 & e_3 & -e_2 & -e_1 \\ -e_3 & e_4 & e_1 & -e_2 \\ e_2 & -e_1 & e_4 & -e_3 \\ e_1 & e_2 & e_3 & e_4 \end{bmatrix} \begin{bmatrix} \dot{e}_1 \\ \dot{e}_2 \\ \dot{e}_3 \\ \dot{e}_4 \end{bmatrix}. \quad (4.12)$$

While an Euler parameter description is used for simulation and attitude estimation, a modified Rodrigues parameter (MRP) representation of the attitude is used in the control laws. MRPs are more elegant for use in a controller because they are a three parameter representation of attitude. They relate to Euler parameters as shown in Eq. (4.13), (4.14) and (4.15).

$$\sigma_1 = \frac{e_1}{1+e_4} \quad \sigma_2 = \frac{e_2}{1+e_4} \quad \sigma_2 = \frac{e_3}{1+e_4} \quad (4.13)$$

$$e_1 = \frac{\sigma_1}{1+\vec{\sigma}^T\vec{\sigma}} \quad e_2 = \frac{\sigma_2}{1+\vec{\sigma}^T\vec{\sigma}} \quad e_3 = \frac{\sigma_3}{1+\vec{\sigma}^T\vec{\sigma}} \quad e_4 = \frac{1-\sigma^T\sigma}{1+\vec{\sigma}^T\vec{\sigma}} \quad (4.14)$$

MRPs have a singularity that exists at a rotation of 360 degrees corresponding to $e_4 = -1$. To deal with this singularity Schaub and Junkins[15] introduce shadowed MRPs which represent a rotation in the opposite direction to the same orientation, as given in Eq. (4.15)

$$\sigma_1 = \frac{-e_1}{1 + e_4} \quad \sigma_2 = \frac{-e_2}{1 + e_4} \quad \sigma_2 = \frac{-e_2}{1 + e_4}. \tag{4.15}$$

The shadowed MRPs are used when $|e|$ is greater than one.

Chapter 5

Reaction Wheel Control

The reaction wheel controller, based on Lyapunov's direct method, was developed by Schaub and Junkins[15]. For completeness, it is presented below.

The controller development starts with the positive definite, radially unbounded, Lyapunov function shown in Eq. (5.1).

$$V(\vec{\sigma}, \delta\vec{\omega}) = \frac{1}{2}\delta\vec{\omega}^T \mathbf{I} \delta\vec{\omega} + 2K ln(1 - \vec{\sigma}^T\vec{\sigma}) \tag{5.1}$$

where $\delta\vec{\omega}$ is the error in absolute angular velocity, $\vec{\sigma}$ is the MRP representation of the rotation from the desired attitude to the actual attitude, and K is a scalar gain. The derivative of Eq. (5.1) is given in Eq. (5.2)

$$\dot{V}(\vec{\sigma},\delta\vec{\omega}) = \delta\vec{\omega}^T\mathbf{I}\frac{d^B}{dt}\delta\vec{\omega} + \delta\vec{\omega}^T K\vec{\sigma} \tag{5.2}$$

where $\frac{d^B}{dt}\vec{\omega}$ represents the derivative taken with respect to the body frame which is equal to $\dot{\vec{\omega}} - \dot{\vec{\omega}}_r + \vec{\omega} \times \vec{\omega}_r$.

According to Lyapunov's direct method, to ensure stability, the derivative of Eq. (5.1) must be negative. Thus, Eq. (5.2) is set equal to a negative definite function as shown in Eq. (5.3)

$$\dot{V}(\vec{\sigma},\delta\vec{\omega}) = -\delta\vec{\omega}^T\mathbf{P}\delta\vec{\omega} \tag{5.3}$$

where $\mathbf{P}$ is a positive definite angular velocity gain matrix. Substituting $\dot{\vec{\omega}} - \dot{\vec{\omega}}_r + \vec{\omega} \times \vec{\omega}_r$ for $\frac{d^B}{dt}\delta\vec{\omega}$ gives eq. (5.4)

$$I\dot{\vec{\omega}} = -K\vec{\sigma} - \mathbf{P}\delta\vec{\omega} + \mathbf{I}(\dot{\vec{\omega}}_r - \vec{\omega} \times \vec{\omega}_r). \tag{5.4}$$

Substituting Eq. (4.5) and (4.6) into Eq. (5.4) gives Eq. (5.5)

$$-\vec{\omega} \times (\mathbf{I}\vec{\omega} + \mathbf{J}(\vec{\omega} + \vec{\Omega}) - \vec{\omega}_r) - \vec{T} + \vec{M} = -K\vec{\sigma} - \mathbf{P}\delta\vec{\omega} + I(\dot{\vec{\omega}}_r - \vec{\omega} \times \vec{\omega}_r). \qquad (5.5)$$

Finally, the motor torque, $\vec{T}$, used to control the satellite can now be solved for:

$$\vec{T} = -\vec{\omega} \times (\mathbf{I}\vec{\omega} + \mathbf{J}(\vec{\omega} + \vec{\Omega}) - \vec{\omega}_r) + \vec{M} + K\vec{\sigma} + \mathbf{P}\delta\vec{\omega} - \mathbf{I}(\dot{\vec{\omega}}_r - \vec{\omega} \times \vec{\omega}_r). \qquad (5.6)$$

5.1 Reaction Wheel Control Simulation

Four different reaction wheel simulations are presented in this section, (1) an inertial attitude change, (2) an inertial attitude tracking, (3) a rate ramp tracking, and (4) a simulated object flyby. These simulations demonstrate the system type number and suitability of the controller for the object tracking task.

The Oculus dynamics of Eq. (4.6) and (4.6) and the controller of Eq. (5.6) were simulated using Simulink and modeled with custom C-coded S-functions. This method of modeling will eventually allow for more direct porting of control laws to C-language satellite flight code.

For all the simulations, the mass properties of Table 5.1 were used. The spin axis inertia for each reaction wheel is 0.00188 kg m^2.

Table 5.1: Reaction Wheel Mass Properties ($kg\ m^2$)

I_{11}	1.61725
I_{22}	1.31325
I_{33}	1.09700
I_{12}	-0.01700
I_{13}	-0.07600
I_{23}	-0.00100

The reaction wheel controller gains were set to $K = 40$ and $\mathbf{P} = 10\mathbf{E}$ to simply demonstrate the controller performance, where $\mathbf{E}$ is the identity matrix. In the future, actual controller gains will be set based on the controller's ability to meet mission performance objectives.

5.1.1 Inertial Attitude Change

The first simulation, analogous to a step response, is an inertial attitude change where the satellite is initially pointing in one direction and changes to point in another.

The satellite is initially at rest and pointing so that the body frame is aligned with the fixed frame. In this position, the Euler parameter attitude is $[0, 0, 0, 1]$. The satellite is then rotated 90 degrees about the b_1 axis to the new Euler parameter attitude of $[\sqrt{.5}, 0, 0, \sqrt{.5}]$. The satellite has a first order-like response with no overshoot as shown in Figure 5.1.

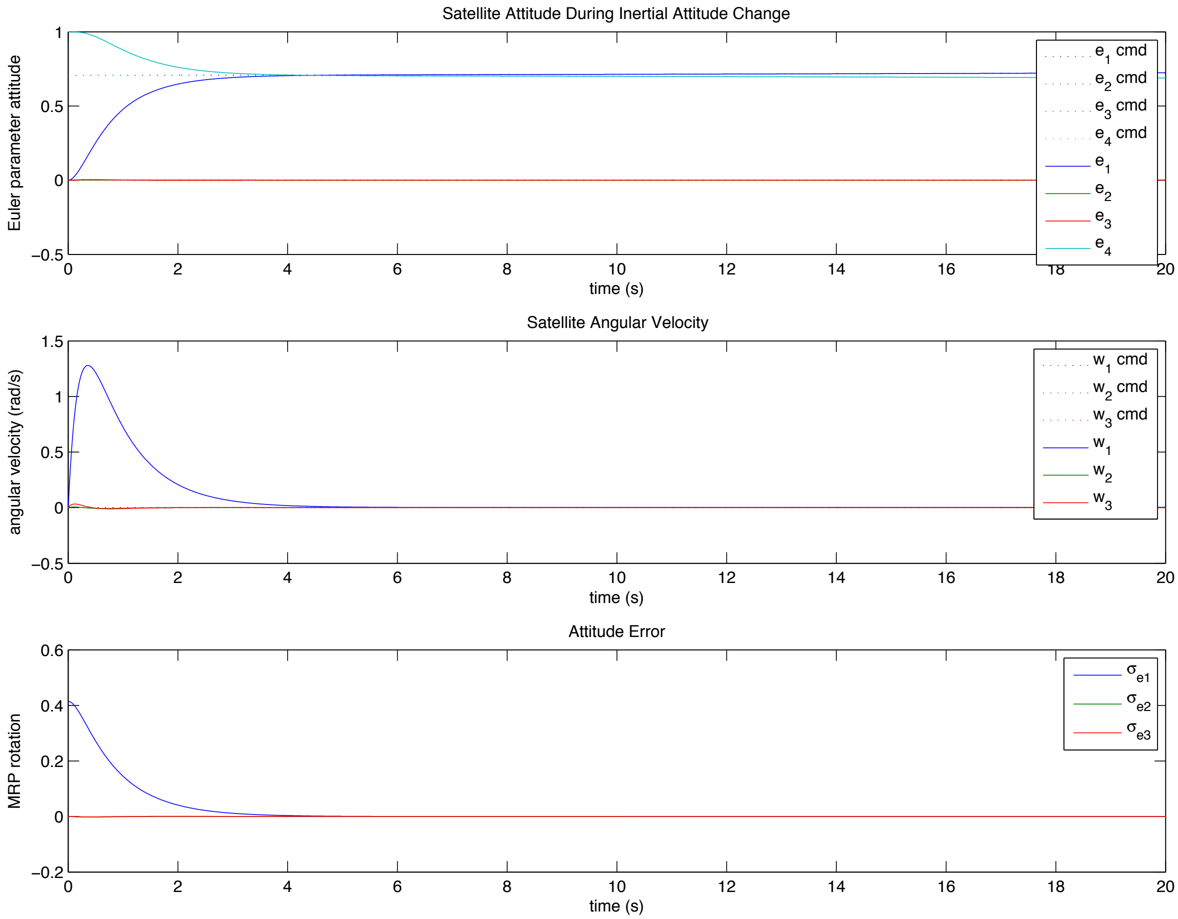

Figure 5.1: Simulation results of the reaction wheel controller demonstrating a single-axis rotation.

All controller simulation results are presented in the same format. In the first plot, the commanded Euler parameter attitude is displayed using dashed lines while, the actual attitude of the satellite is displayed using the solid lines. In the second plot, the commanded and actual angular velocity are presented. Lastly, the attitude error, represented as a MRP, is displayed.

Next, a three-axis maneuver is considered. The satellite was initially at rest and aligned with the fixed frame. The satellite was commanded to the Euler parameter attitude of $[\sqrt{.3}, -\sqrt{.4}, \sqrt{.1}, -\sqrt{.2}]$. Again, there is a first order-like response as shown in Figure 5.2.

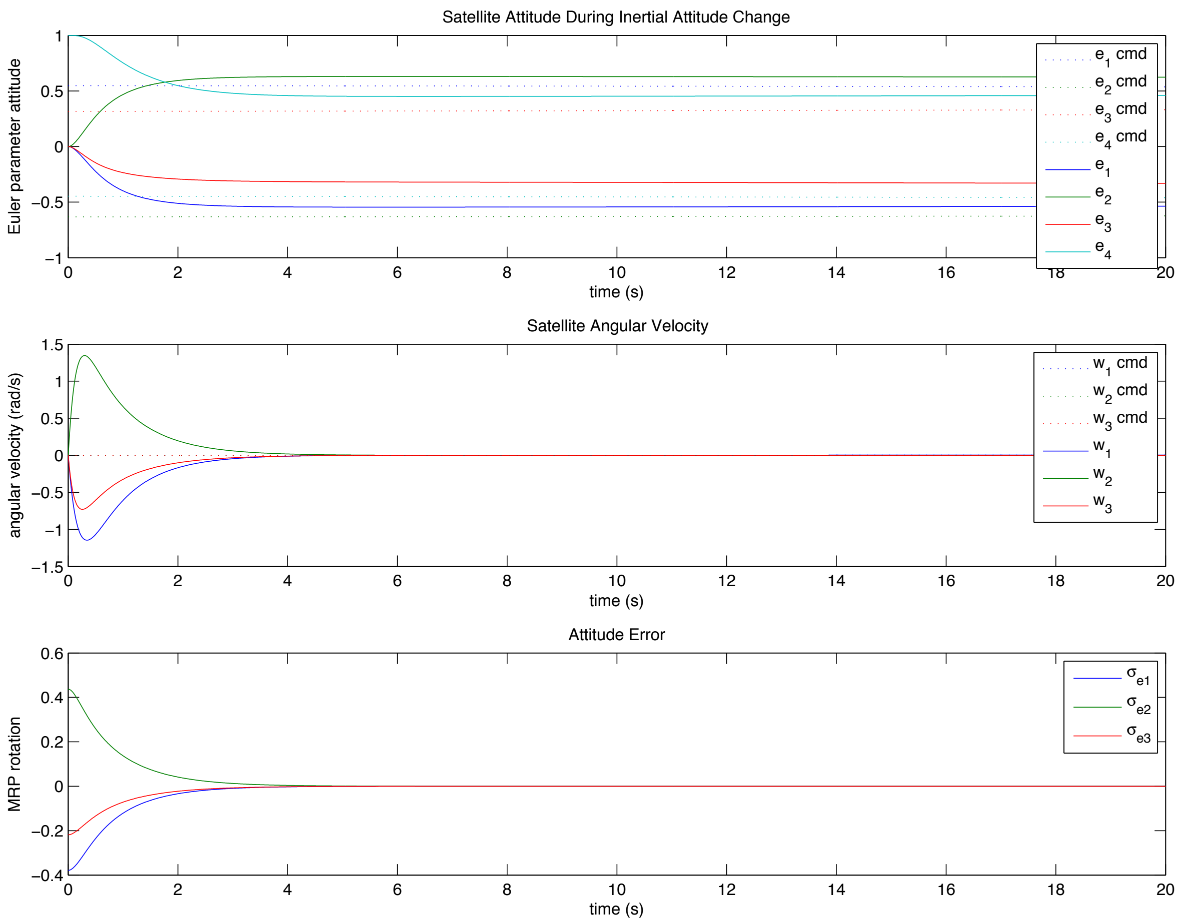

Figure 5.2: Simulation results of the reaction wheel controller demonstrating a three-axis rotation.

This three-axis rotation demonstrates the use of shadowed MRPs. At the end of the simulation, the Euler parameter attitude representation of the satellite does not match the Euler parameter that was used as a command to the controller. The bottom plot confirms the final attitude was correct by showing the error goes to zero. The difference between the final attitude representation and the command attitude representation is the result of the shadowed MRPs used by the controller.

5.1.2 Inertial Attitude Tracking

The ability of the satellite to track a constant rate and change inertial attitude is simulated next. In these simulations the satellite starts at rest. In this first tracking simulation the satellite is commanded to spin at .3 rad/s around the b_1 axis.

Within a few seconds, the satellite catches up with the desired spin rate and has a pointing error of approximately zero as shown in Figure 5.3. From this, it can be inferred that the system type is two or greater.

Next, rate tracking about all three-axes is considered. The satellite was commanded to spin at .3 rad/s about the body x-axis, -.4 rad/s about the body y-axis and .1 rad/s about the body z-axis. The results are shown in Figure 5.4 and match the results of the single-axis rate tracking.

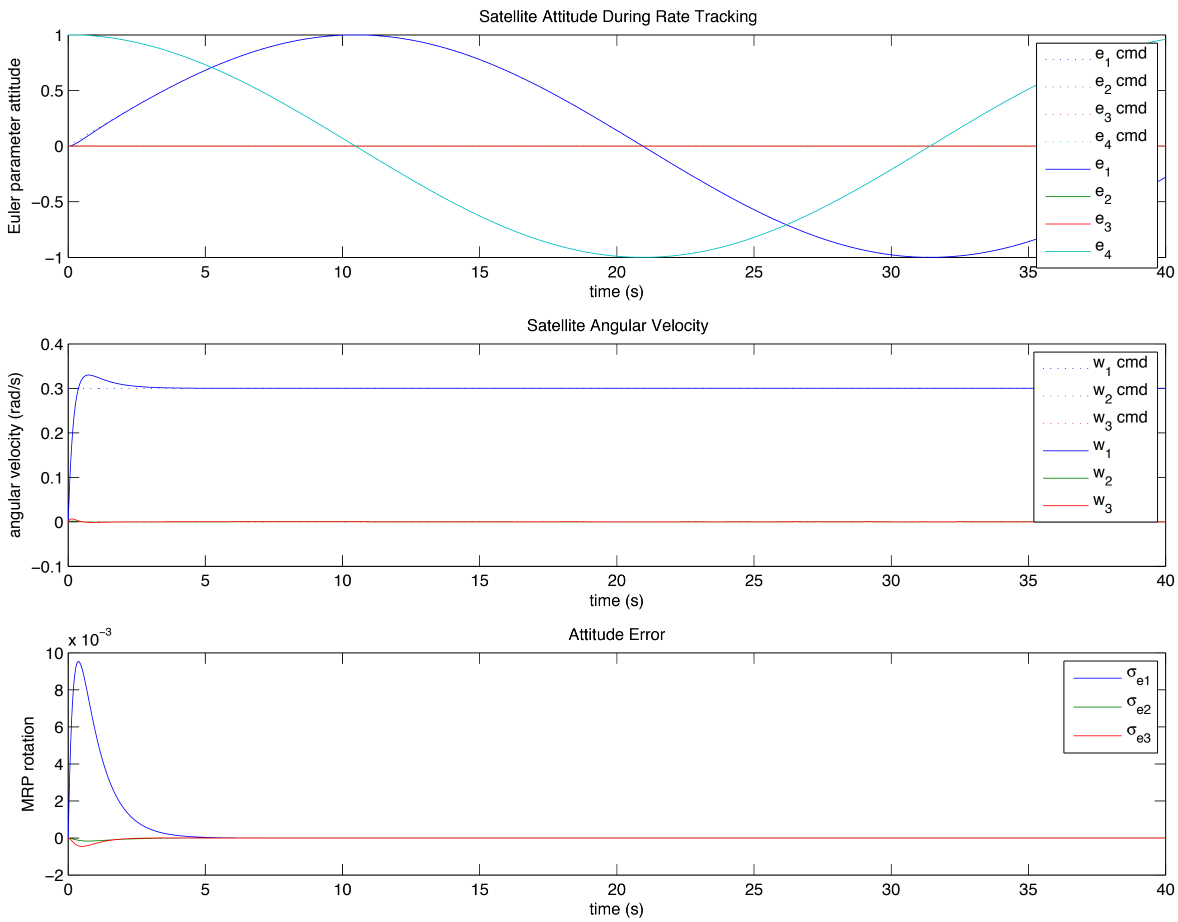

Figure 5.3: Simulation results of the reaction wheel controller demonstrating single-axis rate tracking.

5.1.3 Inertial Attitude Acceleration

To confirm the system type, a simulation with constant acceleration was completed. The simulation results for this are shown in Figure 5.5. From the results of the constant acceleration simulation, it can be observed in the bottom MRP plot that there is a constant offset in attitude. Because this offset occurs for a constant acceleration

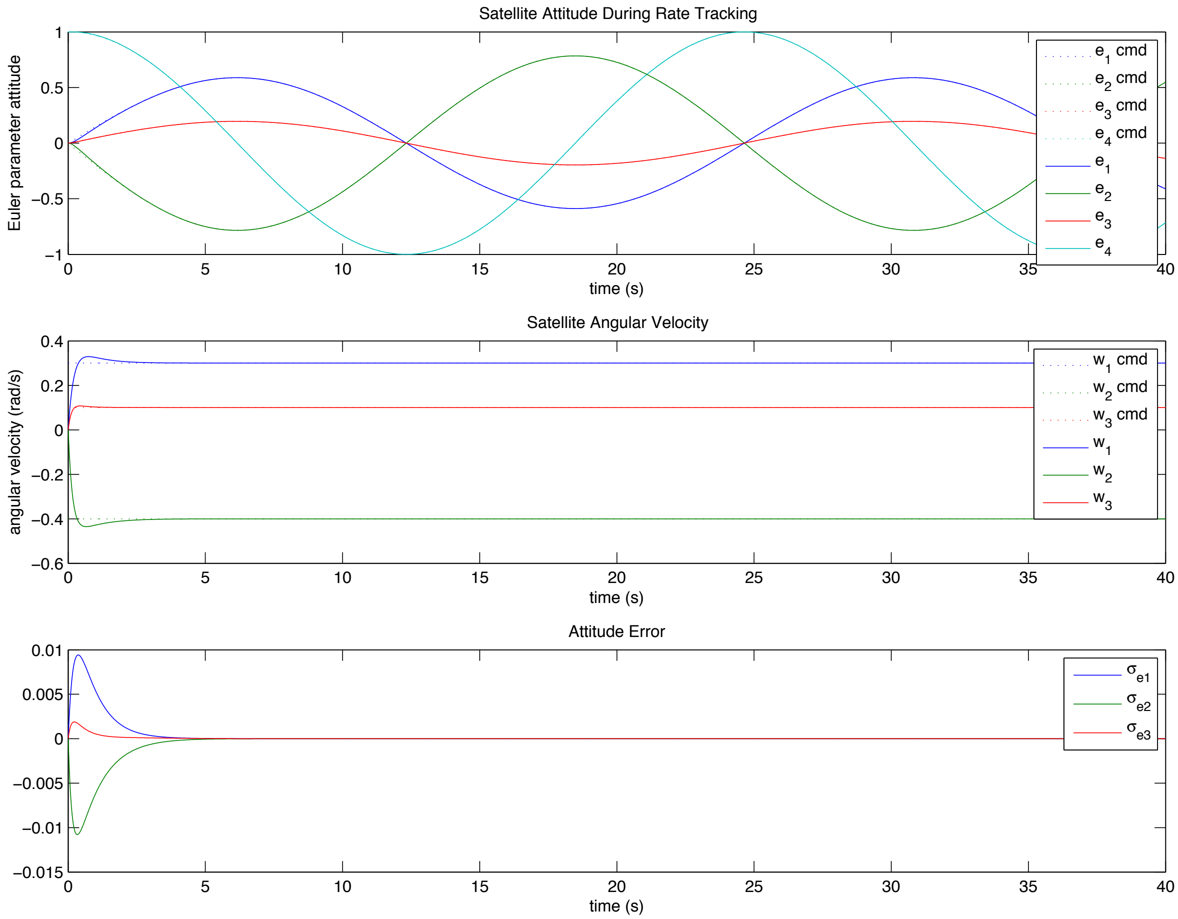

Figure 5.4: Simulation results of the reaction wheel controller demonstrating three-axis rate tracking.

but not for a constant velocity, the system type is two. Because the system type is two, some error is expected during object tracking because the attitude necessary to track resident space objects (RSOs) will require more than constant velocity tracking.

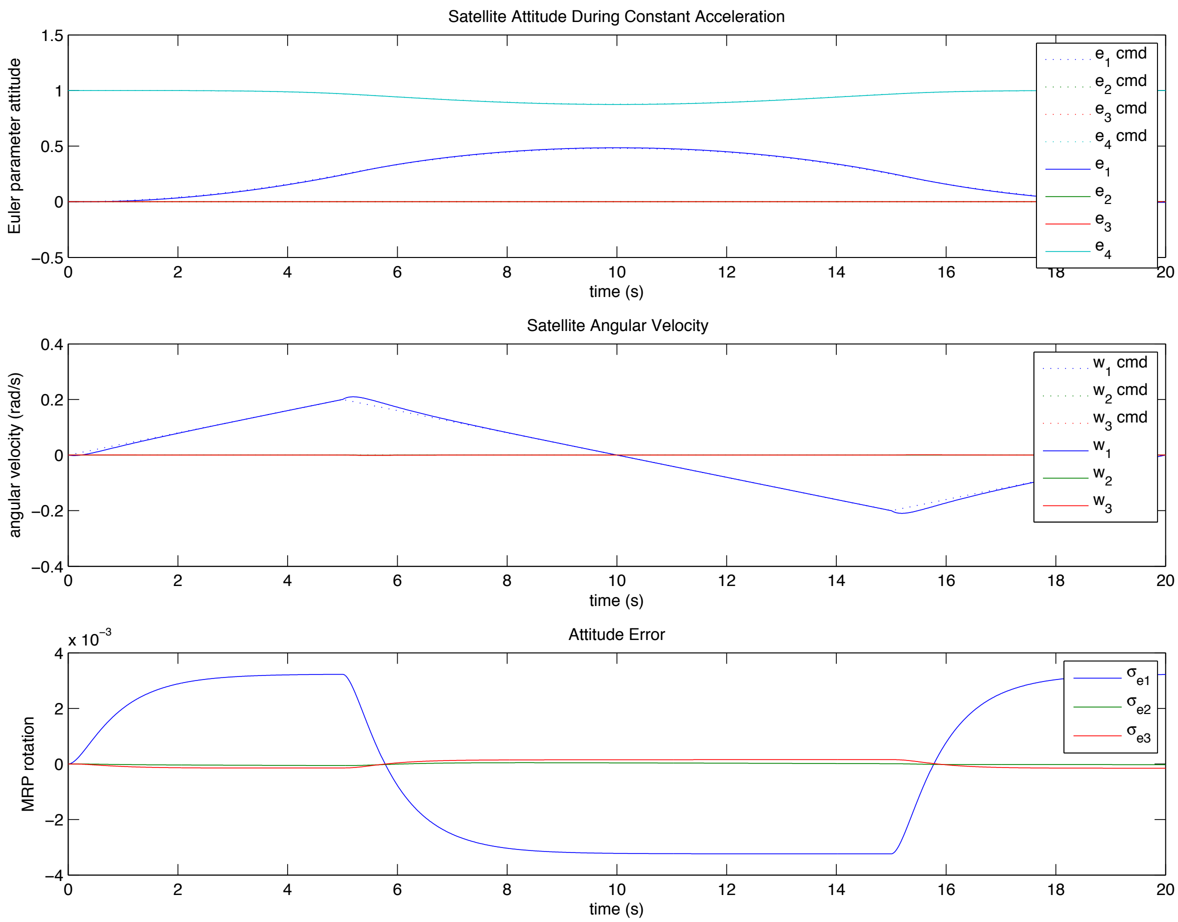

Figure 5.5: Simulation results of the reaction wheel controller demonstrating constant acceleration about one axis

5.1.4 Simulated Flyby

The final simulation case is a flyby. The flyby illustrates the attitude rates necessary to track an object that starts at a position of $[0, 10, 1]$ and moves in a straight line and at a constant velocity to a position of $[0, -10, 1]$ in two minutes. This is the same as having an object 1 km from the satellite moving by the satellite at 600 km/h.

Because the system is type two, the satellite is able to track systems with zero acceleration without steady state error. Tracking non-zero accelerations results in pointing errors in the attitude with the greatest error occurring where there is the greatest acceleration.

Figure 5.6 shows the results from the flyby simulation. As expected, the attitude error was greatest when the magnitude of the slope of the absolute angular velocity was the greatest, at approximately 56 and 62 seconds.

The maximum error in this test case is less than 0.4 degrees. It should be noted that the expected field of view on the Oculus NFOV imager is 8 degrees; thus the 0.4 degree error is sufficient to keep the imaging target within the field of view.

5.2 Stewart Platform Demonstration

To further prove and demonstrate the reaction wheel control system, simulations integrated with a hardware-in-the-loop test bed were conducted.

The Stewart platform, a six-degree-of-freedom rotation/translation table, was chosen as the test bed for the Oculus. Only the rotational capabilities of the platform were used for simulating the Oculus' attitude control system.

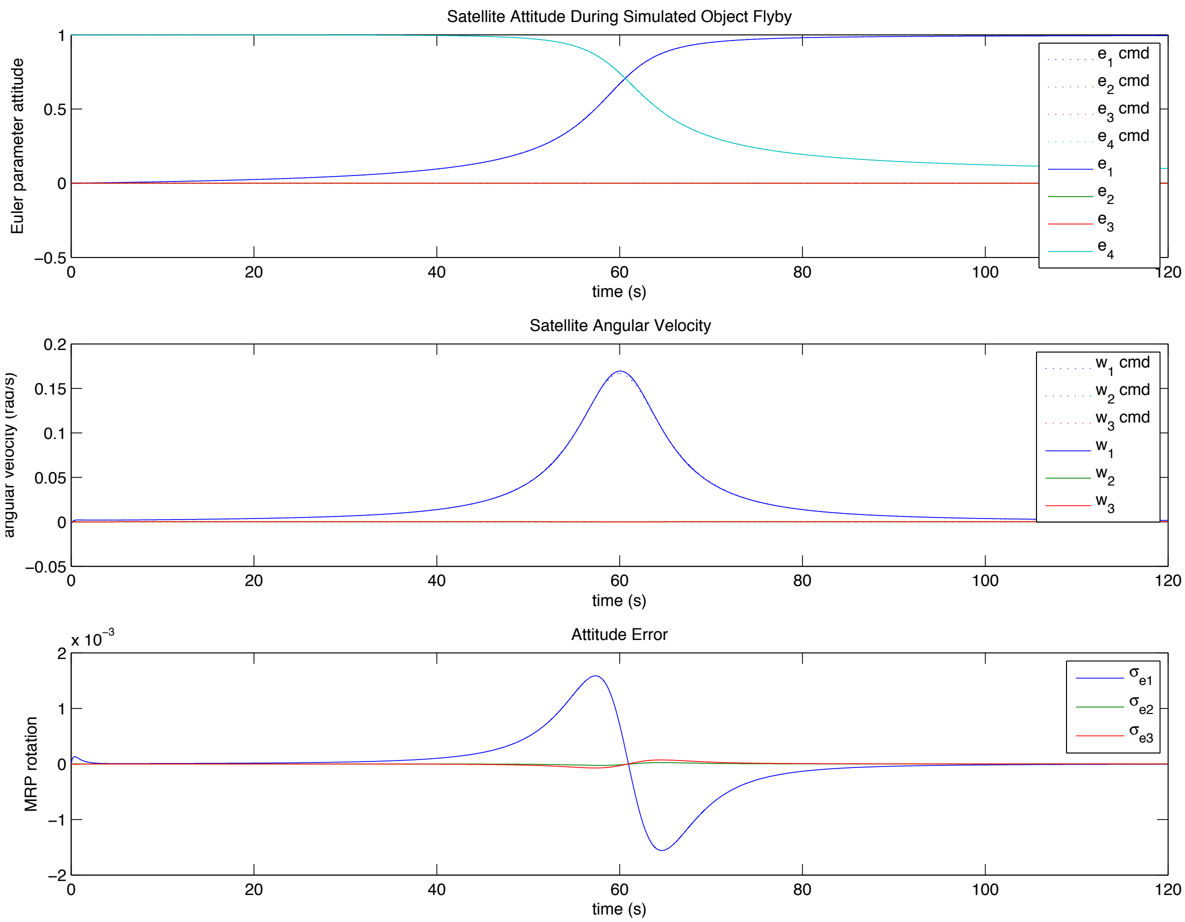

Figure 5.6: Simulation results of the reaction wheel controller demonstrating simulated flyby tracking

The Stewart platform is a parallel manipulator that consists of an upper and lower surface connected by six legs as shown in Figure 5.7. The orientation of the upper platform relative to the lower platform is achieved by changing the lengths of the legs of the platform. The forward and inverse kinematics of the Stewart platform are presented by Huang[3].

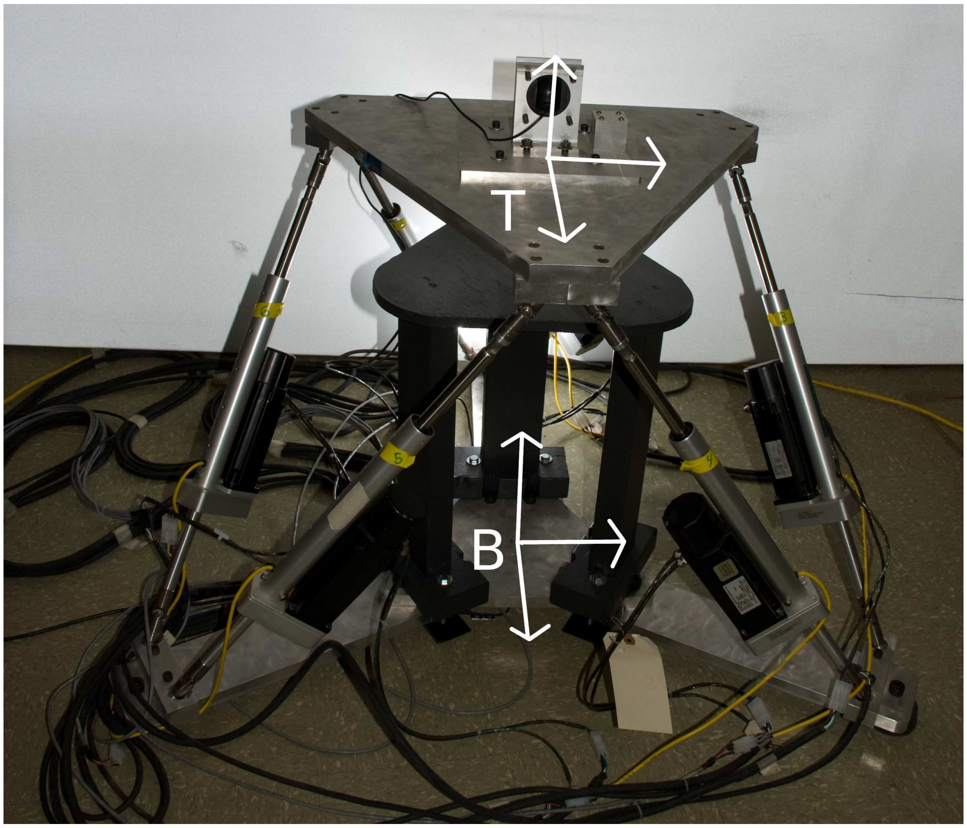

Figure 5.7: Stewart platform setup for attitude control simulation with visual servoing

The first step in calculating the leg lengths using the Euler parameter attitude is to assign coordinate frames to the base, B, and the top, T, of the platform. Using these coordinate frames, vectors from the origin to each attachment point are found.

Next, the attachment point vectors of the top plate in the T frame are rotated using the rotation matrix in Eq. (5.7).

$$
\mathbf{R} = \begin{bmatrix} e_4^2 + e_1^2 - e_2^2 - e_3^2 & 2(e_1e_2 + e_4e_3) & 2(e_1e_2 - e_4e_2) \\ 2(e_1e_2 - e_4e_3) & e_4^2 - e_1^2 + e_2^2 - e_3^2 & 2(e_2e_3 + e_4e_1) \\ 2(e_1e_2 + e_4e_2) & 2(e_2e_3 - e_4e_1) & e_4^2 - e_1^2 - e_2^2 + e_3^2 \end{bmatrix} \tag{5.7}
$$

The vector from the base platform to the top platform, when the platform is at its zero position, is added to the rotated top platform attachment point vectors. If a translation, in addition to a rotation, was desired, it would also be added at this point. The results of these calculations are vectors to the top plate attachment points represented in the base frame.

To get the leg length measurements, the vector to the base attachment point is subtracted from the respective top attachment point and the magnitude of the resulting vector is found. The Stewart platform uses a proportional-derivative (PD) controller to control the leg lengths.

5.3 Model-Hardware Integration

The Stewart platform utilized the satellite and reaction wheel dynamics simulation to command its orientation. Figure 5.8 shows the hardware in-the-loop setup used with the Stewart platform.

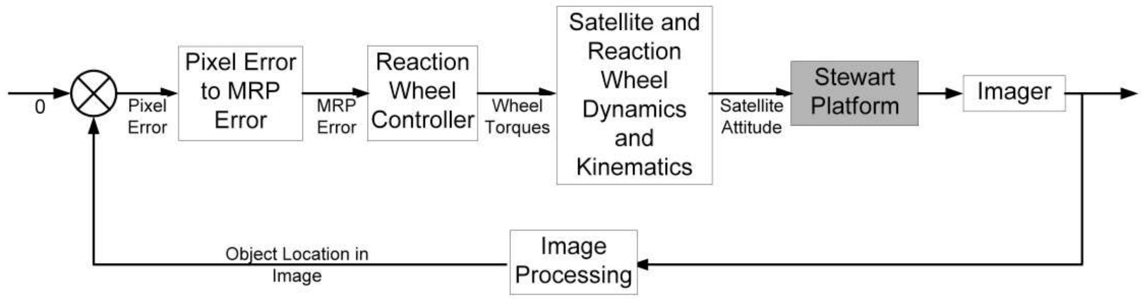

Figure 5.8: Stewart platform hardware-in-the-loop feedback diagram

Basic imaging software was used to determine the error in the pixel position of the target object relative to the center of the field of view of the imager. This done by identifying the largest area that was brighter than a calibratable brightness. The pixel error is converted to an angular error which is fed to the reaction wheel controller. The final imaging software that will be used for flight is currently being developed by an Oculus team member.

The reaction wheel controller calculates the reaction wheel torques required to drive the pixel error to zero. The satellite and reaction wheel dynamics and kinematics simulates the rotation of the satellite based on these torques. The result of the simulated satellite and reaction wheels is an Euler parameter representation of the satellite attitude. The Stewart platform uses the Euler parameter representation of attitude to orient the vision system attached to it.

The hardware-in-the-loop setup was able to demonstrate the reaction wheel controller being used in a visual servoing application. The stewart platform hardware in the loop demonstration allows for greater confidence in the control system developed for the Oculus. In the future, this setup will be used for flight hardware and software integration and testing.

Chapter 6

Magnetic Torque Rod Control

Magnetic torque rod attitude control is used on the Oculus in addition to reaction wheel control to manage stored momentum of the reaction wheels and orient the satellite. The simplest way to accomplish this momentum management is to force the wheel speeds to zero when precise attitude control is not necessary such as when the Oculus is orbiting in an idle state. Forcing the reaction wheels to zero will transfer the momentum stored in the wheels to the satellite and will result in general three-axis rotation of the satellite, which is removed by the magnetic torque rods. To accomplish the desaturation and general orientation, three-axis magnetic torque rod control is necessary.

Magnetic torque rod control is possible because when current flows through a coil of wire a magnetic moment, $\vec{u}_m$, is generated. This magnetic moment in conjunction with earth's magnetic field, $\vec{b}(t)$, generates a torque on the satellite. The cross product of the magnetic moment and the magnetic field represents the generated torque $\vec{T}_m$ on the satellite. This relationship is described in Eq. (6.1)

$$\vec{T}_m = \vec{u}_m \times \vec{b}(t). \tag{6.1}$$

If $\vec{b}(t)$ is time invariant, such as when the satellite is not changing position relative to the earth's magnetic field, the angular velocity about the magnetic field vector cannot be controlled. For any given magnetic field vector, torque can not be generated about that vector. This can easily be demonstrated using the vector $[1, 0, 0]$ as the magnetic field vector and $[1, 1, 1]$ as the magnetic moment. When the cross product is taken of these two vectors, the resultant vector, $[0, 1, -1]$, does not provide any torque around the magnetic field vector even though all the torque rods have current flowing through them generating a magnetic moment.

The satellite orbits the earth, resulting in a magnetic field that changes with time. As a result, the vector about which torque can not be applied does not remain constant. The time varying magnetic field allows for the system to be controllable.

6.1 Magnetic Torque Rod Controller Design

During magnetic torque rod control the reaction wheels will be commanded to spin at a constant angular velocity relative to the body frame or commanded to spin at zero angular velocity relative to the body frame, effectively desaturating the reaction wheels, before magnetic torque rod control commences. The following analysis was completed for fully desaturated reaction wheels with zero spin. This allows for the simplification of the equations of motion from Eq. (4.5), as shown in Eq. (6.4)

$$\vec{M} = (\mathbf{I} + \mathbf{J})\dot{\vec{\omega}} + \vec{\omega} \times ((\mathbf{I} + \mathbf{J})\vec{\omega}) \tag{6.2}$$

where

$$\vec{M} = \vec{M}_{disturbance} + \vec{M}_{torquerods} \tag{6.3}$$

and

$$\vec{M}_{torquerods} = \vec{b}(t) \times \vec{M}_{desired} \times \vec{b}(t). \tag{6.4}$$

Lyapunov's direct method is used to design the controller used during magnetic torque rod control. Under normal circumstances this design method would guarantee stability of the controller. However, the magnetic torque rods force us to stray from the control law designed using Lyapunov's direct method resulting in a controller that we no longer analytically prove stability for using the same techniques. Showing analytical proof of stability of this controller is outside the scope of this work.

Consider the following positive definite, radially unbounded, Lyapunov function shown in Eq. (6.5)

$$V = \frac{1}{2}\delta\vec{\omega}^T[I + J]\delta\vec{\omega} + 2Kln(1 + \vec{\sigma}\vec{\sigma}^T) \tag{6.5}$$

where $\delta\vec{\omega}$ is the error in angular velocity and $\vec{\sigma}$ is the desired attitude relative to the current attitude. The derivative of V is shown in Eq. (6.6)

$$\dot{V} = \delta\vec{\omega}^T\left([\mathbf{I} + \mathbf{J}]\frac{^Bd}{dt}(\vec{\delta}\omega) + K\vec{\sigma}\right). \tag{6.6}$$

For stability the derivative of V must be at least negative semidefinate. To make the derivative function negative semidefinite it is set equal to the function in Eq. (6.7)

$$\dot{V} = -\delta\vec{\omega}^T \mathbf{P} \delta\vec{\omega} \tag{6.7}$$

resulting in Eq (6.8)

$$[\mathbf{I} + \mathbf{J}] \frac{^B d}{dt}(\delta\vec{\omega}) + \mathbf{P}\delta\vec{\omega} + K\vec{\sigma} = 0. \tag{6.8}$$

Substituting in $\dot{\vec{\omega}} - \dot{\vec{\omega}}_r + \vec{\omega} \times \vec{\omega}_r$ for $\frac{d^B}{dt}\delta\vec{\omega}$ and Eq. (6.4) yields the following control law for a fully actuated system shown in Eq. (6.9).

$$\vec{M}_{desired} = \vec{\omega} \times ([\mathbf{I} + \mathbf{J}]\vec{\omega}) + [\mathbf{I} + \mathbf{J}]\dot{\vec{\omega}}_r - [\mathbf{I} + \mathbf{J}]\vec{\omega} \times \vec{\omega}_r - K\vec{\sigma} - \mathbf{P}\delta\vec{\omega} \tag{6.9}$$

This equation can be further simplified by removing the non working term, $\vec{\omega} \times ([\mathbf{I} + \mathbf{J}]\vec{\omega})$. During magnetometer control, the angular velocity command will be set to a small constant value or zero. As a result, the acceleration command term is zero and the $[\mathbf{I} + \mathbf{J}]\dot{\vec{\omega}}_r$ can be removed. Finally, the cross product term, $[\mathbf{I} + \mathbf{J}]\vec{\omega} \times \vec{\omega}_r$ can be removed because it is not multiplied by a gain, and is expected to be very small compared to the remaining terms as the result of a small commanded $\vec{\omega}_r$. Eq. (6.10) shows the simplified control law

$$\vec{M}_{desired} = -K\vec{\sigma} - \mathbf{P}\delta\vec{\omega} \tag{6.10}$$

where $\vec{M}$ is the ideal torque to apply to the satellite. Because the magnetic torque rods are unable to apply torque in any arbitrary direction, the equation for the part of the desired torque that can be applied to the satellite is shown in Eq. 6.11.

$$\vec{T}_m = \vec{b}(t) \times (-K\vec{\sigma} - \mathbf{P}\delta\vec{\omega}) \times \vec{b}(t) \tag{6.11}$$

where the magnetic moment generated by the satellite's magnetic torque rods is shown in Eq. (6.12)

$$\vec{u}_m = \vec{b}(t) \times (-K\vec{\sigma} - \mathbf{P}\delta\vec{\omega}). \tag{6.12}$$

The magnetic torque rods on the Oculus are orientated such that each of the vectors which a coil wraps around corresponds to a body axis vector. Each element of $\vec{u}_m$ is the magnetic moment generated by the magnetic torque rod which is oriented so that the coil wraps around the associated axis. The magnetic moment generated by a rod is proportional the current in the coil for that rod.

6.2 Magnetic Torque Rod Stability Analysis

Instead of showing analytical stability of the controller, a short conceptual explanation of the difficultly of showing analytical stability will be given, along with simulation results demonstrating the likelihood of stability for the controller.

Showing stability of this magnetic torque rod controller analytically is far more complicated than showing stability for a system that has full actuation at any point in time. One method that could be used to show stability would be to model the position of the satellite and using this position, determine the magnetic field resulting from a simple dipole model of the Earth's magnetic field. Because of the increased complexity of the system, it is not practical to search for a suitable Lyapunov function and as a result this method is impracticable.

The method used by Astolfi and Lovera [1] to show stability for their Euler parameter based controller is generalized averaging. This same technique can not be applied to the MRP-based controller because generalized averaging depends on the system equations, $f(t, x, \epsilon)$, being continuous and bounded, which is not the case for MRPs which have a singularity at a rotation of 360 degrees. This singularity goes away with the use of the shadowed MRP but is now discontinous.

The result of Alessandro Astolfi and Marco Lovera analysis of their Euler parameter based controller indicates probable stability for the MRP-based controller used on the Oculus based on the relationship of Euler parameters and MRPs.

6.3 Magnetic Torque Rod Control Simulation

The magnetic torque rod controller is simulated using Simulink with custom S-functions for the controller, a magnetic field model, and the satellite dynamic equations.

As shown in Figure 6.1, the magnetic torque rod controller is capable of regulating the satellite absolute angular velocity. The angular velocity in this simulation starts at .2 rad/s/axis, which is the expected initial angular velocity as a result of launch, and in less than an orbit is reduced to nearly zero. At this point the satellite can either be switched back to reaction wheel control for fast and precise movement, or as shown in the simulation, the magnetic torque rods can be used to orient the satellite.

Actual performance results of the satellite will vary from the response shown as a result of the torque rod design and controller gain calibration but is expected to be able to stabilize the satellite within the requirement of one hour.

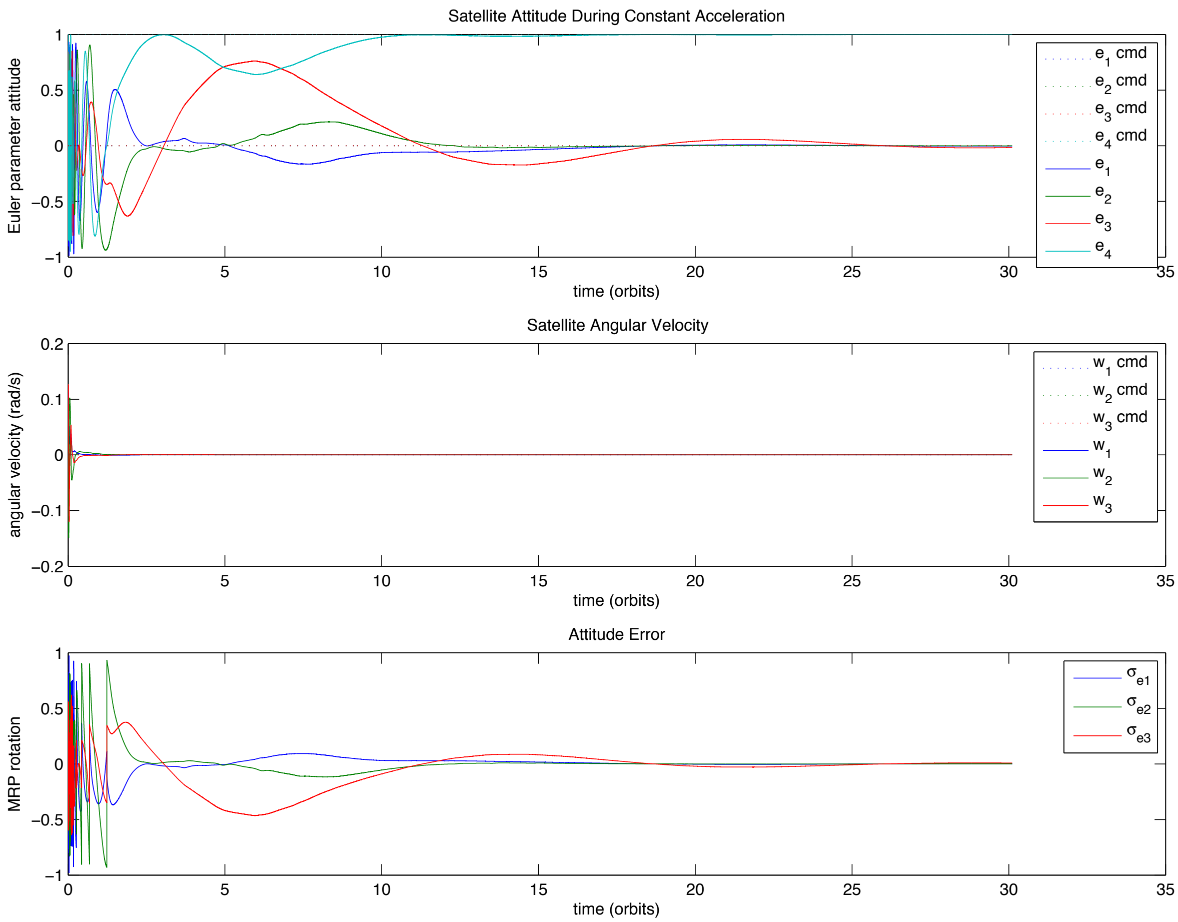

Figure 6.1: Simulation results demonstrating the magnetic torque rod controller.

Chapter 7

Attitude Estimation

The attitude estimator is used to determine the orientation of the Oculus based on readings from onboard sensors and models. The simplest attitude estimator that could be implemented using the Oculus hardware is an attitude rate integrator using gyroscope measurements. If perfect readings of the satellite absolute angular velocity and initial position were available the basic attitude integrator would give a perfect attitude estimate. Unfortunately, perfect readings are not available and a basic attitude rate integrator would give an erroneous attitude estimate. To deal with the angular velocity error and imperfect initial position, a better attitude estimator is necessary.

The Oculus is also equipped with a magnetometer which is used to read the magnetic field. Single measurements from the magnetometer alone are insufficient to determine the orientation because the rotation about the magnetic field vector is unmeasurable.

The Oculus' attitude estimator utilizes both the magnetometer and gyroscope measurements, along with the ephemeris data and time, and is implemented using the nonlinear extension of the Kalman Filter, the Extended Kalman Filter (EKF).

Simulation results are provided for two EKF attitude estimators developed in sections 7.1 and 7.2. These results demonstrate proper functioning of the filter, not performance. At the time of writing, noise models for the sensors and actuators were unavailable and as a result the noise models used for simulation are may not be representative of the actual sensors and actuators. All simulations use the system dynamics and reaction wheel closed loop controller to generate the satellite attitude. For each attitude estimator simulation the same simulation setup and noise covariance were used. A simulation example of the erroneous attitude as a result of basic integration is provided in Figure (7.1) as a comparison for other attitude estimators developed in this chapter.

Each set of simulation results in this chapter follow the same format. In the first plot, the true attitude of the satellite is presented using Euler parameters. In the second plot, the estimated attitude of the satellite is presented, again using Euler parameters. The final plot of Figure 7.2 shows the sum of the Euler parameter errors squared.

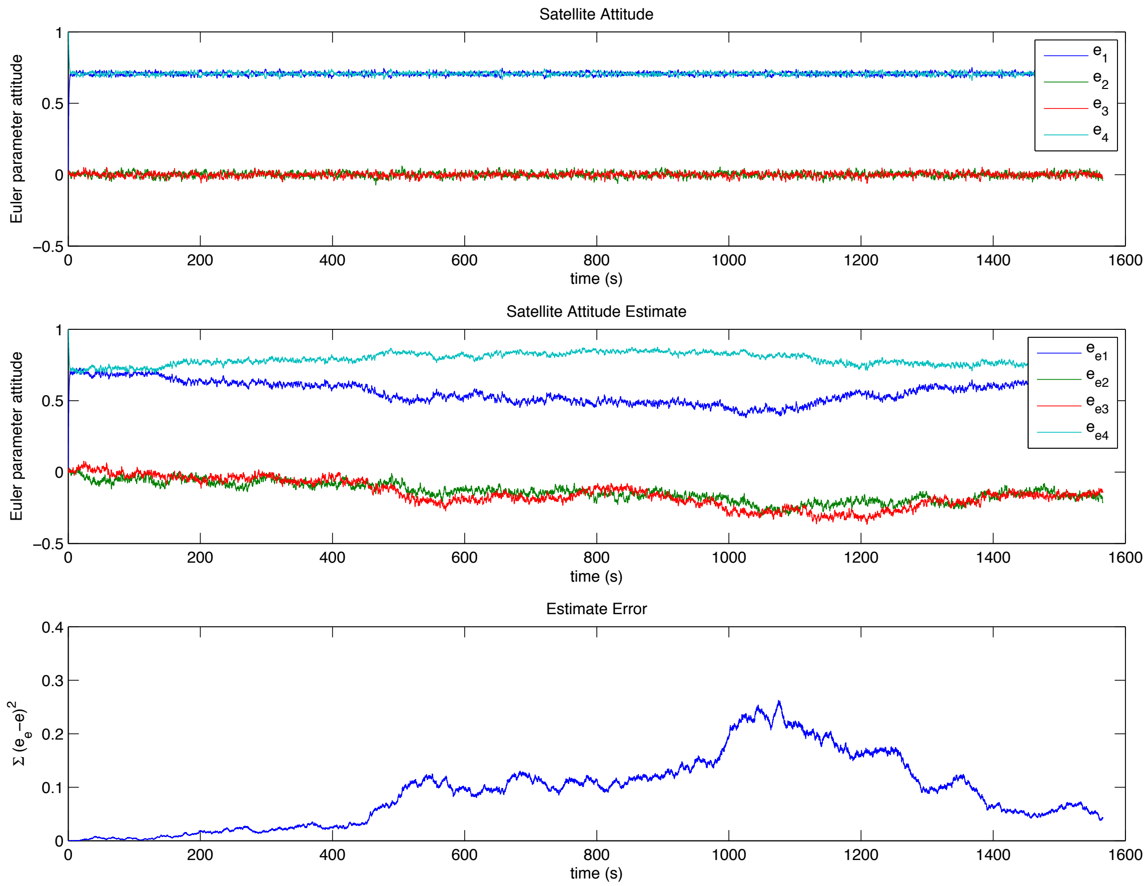

Figure 7.1: Simulation results of the estimated satellite attitude using only the kinematic equations.

The attitude estimator on the Oculus satellite is implemented at a fixed sample rate which will be determined based on available computing resources. The general form of the nonlinear discrete time system that will be used in the filter development is shown in Eq. (7.1) and Eq. (7.2)

$$\vec{x}(k+1) = f(\vec{x}(k), \vec{u}(k), \vec{w}(k), k) \tag{7.1}$$

$$\vec{y}(k) = g(\vec{x}(k), k) + \vec{v}(k) \tag{7.2}$$

where $\vec{x}$ is the state vector, $\vec{u}$ is the input vector, $\vec{w}$ is process noise vector, $\vec{y}$ is the measurement vector, and $\vec{v}$ is the measurement noise vector.

The form of the Extended Kalman filter used on the Oculus is shown in Eq. (7.3) to Eq. (7.7)[4]

$$\mathbf{K}(k) = \mathbf{P}(k)^{-}\mathbf{H}(k)^{T}(\mathbf{H}(k)\mathbf{P}(k)^{-}\mathbf{H}(k)^{T} + \mathbf{R})^{-1} \tag{7.3}$$

$$\hat{\vec{x}}(k) = \hat{\vec{x}}(k)^{-} + \mathbf{K}(k)(\vec{y}(k) - g(\hat{\vec{x}}(k)^{-}, k)) \tag{7.4}$$

$$\mathbf{P}(k) = (I - \mathbf{K}(k)\mathbf{H}(k))\mathbf{P}(k)^{-} \tag{7.5}$$

$$\hat{\vec{x}}(k+1)^{-} = f(\hat{\vec{x}}(k), \vec{u}(k), k) \tag{7.6}$$

$$\mathbf{P}(k+1)^{-} = \mathbf{\Phi}(k)\mathbf{P}(k)\mathbf{\Phi}(k)^{T} + \mathbf{\Gamma}(k)\mathbf{Q}\mathbf{\Gamma}(k)^{T}. \tag{7.7}$$

where $\hat{x}$ is the estimated state vector, $\mathbf{K}$ is the Kalman gain matrix, $\mathbf{P}$ is the error covariance matrix, $\mathbf{Q}$ is the process noise covariance matrix, $\mathbf{R}$ is the measurement noise covariance matrix and the matrices,

$$\mathbf{\Phi}(k) = \left.\frac{\partial f(\vec{x}(k), \vec{u}(k), \vec{w}(k)k)}{\partial \vec{x}(k)}\right|_{\vec{x}(k)=\hat{\vec{x}}(k), \vec{u}(k)=\vec{u}(k), \vec{w}(k)=0} \tag{7.8}$$

$$\mathbf{\Gamma}(k) = \left.\frac{\partial f(\vec{x}(k), \vec{u}(k), \vec{w}(k)k)}{\partial \vec{w}(k)}\right|_{\vec{x}(k)=\hat{\vec{x}}(k), \vec{u}(k)=\vec{u}(k), w(k)=0} \tag{7.9}$$

$$\mathbf{H}(k) = \left.\frac{\partial g(\vec{x}(k), k)}{\partial \vec{x}(k)}\right|_{\vec{x}(k)=\hat{\vec{x}}(k)} \tag{7.10}$$

are the linearized state and measurement equations around the operating point. The selection of the noise covariance matrices should be completed by analyzing the noise characteristics of the sensors and actuators.

The available sensors and actuators on the satellite allow for the satellite attitude estimator to be implemented using two different configurations. The first configuration uses both the dynamics and kinematics of the system. The second, simpler, configuration of the Kalman filter uses only the satellite kinematics. For both systems, the continuous system is made into a discrete time system using Euler method as shown in Eq. (7.11)

$$\vec{x}(k+1) = \vec{x}(k) + h(f(\vec{x})) \tag{7.11}$$

where h is the step size.

7.1 Kinematic and Dynamic Attitude Estimator

The first Kalman filter implementation is for the system discribed through the dynamic and kinematic equations of the satellite. The Oculus' system dynamic and kinematic equations, shown in Eq. 7.12 to Eq. 7.14, are used to generate the $\mathbf{\Gamma}$ and $\mathbf{\Phi}$ matrices. The inputs to the system are three moments on the satellite, $\vec{u}_s$, and the three reaction wheel torques, $\vec{L}$.

$$\dot{\vec{\omega}} = \mathbf{I}^{-1}(\vec{L} - \vec{\omega} \times \mathbf{I}\vec{\omega} - \vec{\omega} \times \mathbf{J}(\vec{\omega} + \vec{\Omega}) - \vec{u}_s) \tag{7.12}$$

$$\dot{\vec{\Omega}} = \mathbf{J}^{-1}\vec{u}_s - \mathbf{I}^{-1}(\vec{L} - \vec{\omega} \times \mathbf{I}\vec{\omega} - \vec{\omega} \times \mathbf{J}(\vec{\omega} + \vec{\Omega}) - \vec{u}_s) \tag{7.13}$$

$$\dot{\vec{e}} = \frac{1}{2} \begin{bmatrix} e_4 & e_3 & -e_2 & -e_1 \\ -e_3 & e_4 & e_1 & -e_2 \\ e_2 & -e_1 & e_4 & -e_3 \\ e_1 & e_2 & e_3 & e_4 \end{bmatrix}^{-1} \begin{bmatrix} \omega_1 \\ \omega_2 \\ \omega_3 \\ -c(e_1^2 + e_2^2 + e_3^2 + e_4^2 - 1) \end{bmatrix} \tag{7.14}$$

Baumgarte stabilization is used in the kinematic equation. Baumgarte stabilization in the Kalman filter can be removed by setting the value for c from Eq. (7.14) to zero.

The measurement equations, used to generate the $\mathbf{H}$ matrix, are based on the sensors available on the Oculus. The Oculus is equipped with encoders to read the reaction wheel speeds, $\vec{\Omega}$, a three axis gyroscope to read the absolute angular velocity, $\vec{\omega}$, and a three axis magnetometer to read the magnetic field vector in the body frame, ${}^b\vec{B}$. The magnetic field in the fixed frame, ${}^r\vec{B}$, is calculated from an orbital and magnetic field model. Using these sensors, the first two parts of the output equation are the satellite spin rate and the wheel speed. The final measurement equation is the representation of the magnetic field in the body frame as shown in Eq. (7.15)

$$
{}^b\vec{B} = \begin{bmatrix} e_4^2 + e_1^2 - e_2^2 - e_3^2 & 2(e_1e_2 - e_4e_3) & 2(e_1e_2 + e_4e_2) \\ 2(e_1e_2 + e_4e_3) & e_4^2 - e_1^2 + e_2^2 - e_3^2 & 2(e_2e_3 - e_4e_1) \\ 2(e_1e_2 - e_4e_2) & 2(e_2e_3 + e_4e_1) & e_4^2 - e_1^2 - e_2^2 + e_3^2 \end{bmatrix} {}^r\vec{B} \tag{7.15}
$$

The process noise, denoted by $\vec{w}(k)$, was selected such that it effects all the states of the system and is the same structure as the system inputs. The process noise for the system is added to the reaction wheel torques and the moments on the satellite as shown in Eq. (7.16)

$$
\dot{\vec{\omega}} = \mathbf{I}^{-1}(\vec{L} - \vec{\omega} \times \mathbf{I}\vec{\omega} - \vec{\omega} \times \mathbf{J}(\vec{\omega} + \vec{\Omega}) - (\vec{u}_s + \vec{w}_{1,2,3})) \tag{7.16}
$$

$$
\dot{\vec{\Omega}} = \mathbf{J}^{-1}\vec{u}_s - \mathbf{I}^{-1}((\vec{L} + \vec{w}_{4,5,6}) - \vec{\omega} \times \mathbf{I}\vec{\omega} - \vec{\omega} \times \mathbf{J}(\vec{\omega} + \vec{\Omega}) - (\vec{u}_s + \vec{w}_{1,2,3})) \tag{7.17}
$$

$$\dot{\vec{e}} = \frac{1}{2}\begin{bmatrix} e_4 & e_3 & -e_2 & -e_1 \\ -e_3 & e_4 & e_1 & -e_2 \\ e_2 & -e_1 & e_4 & -e_3 \\ e_1 & e_2 & e_3 & e_4 \end{bmatrix}^{-1} \begin{bmatrix} \omega_1 \\ \omega_2 \\ \omega_3 \\ -c(e_1^2 + e_2^2 + e_3^2 + e_4^2 - 1) \end{bmatrix} \tag{7.18}$$

The measurement noise, denoted by $\vec{v}(k)$, is added directly the measurement variables and is used to represent measurement error by noise. The states, measurements, and inputs are assigned to the variables used in the filter as follows:

$$\begin{bmatrix} x_1 \\ x_2 \\ x_3 \\ x_4 \\ x_5 \\ x_6 \\ x_7 \\ x_8 \\ x_9 \\ x_{10} \end{bmatrix} = \begin{bmatrix} \omega_1 \\ \omega_2 \\ \omega_3 \\ \Omega_1 \\ \Omega_2 \\ \Omega_3 \\ e_1 \\ e_2 \\ e_3 \\ e_4 \end{bmatrix} \quad \begin{bmatrix} y_1 \\ y_2 \\ y_3 \\ y_4 \\ y_5 \\ y_6 \\ y_7 \\ y_8 \\ y_9 \end{bmatrix} = \begin{bmatrix} \omega_1 \\ \omega_2 \\ \omega_3 \\ \Omega_1 \\ \Omega_2 \\ \Omega_3 \\ {}^bB_1 \\ {}^bB_2 \\ {}^bB_3 \end{bmatrix} \quad \begin{bmatrix} u_1 \\ u_2 \\ u_3 \\ u_4 \\ u_5 \\ u_6 \end{bmatrix} = \begin{bmatrix} u_{s1} \\ u_{s2} \\ u_{s3} \\ L_1 \\ L_2 \\ L_3 \end{bmatrix} \tag{7.19}$$

Using this setup, the attitude estimator implemented using both the kinematic and dynamic equations was simulated. The results of this simulation are shown in Figure 7.2)

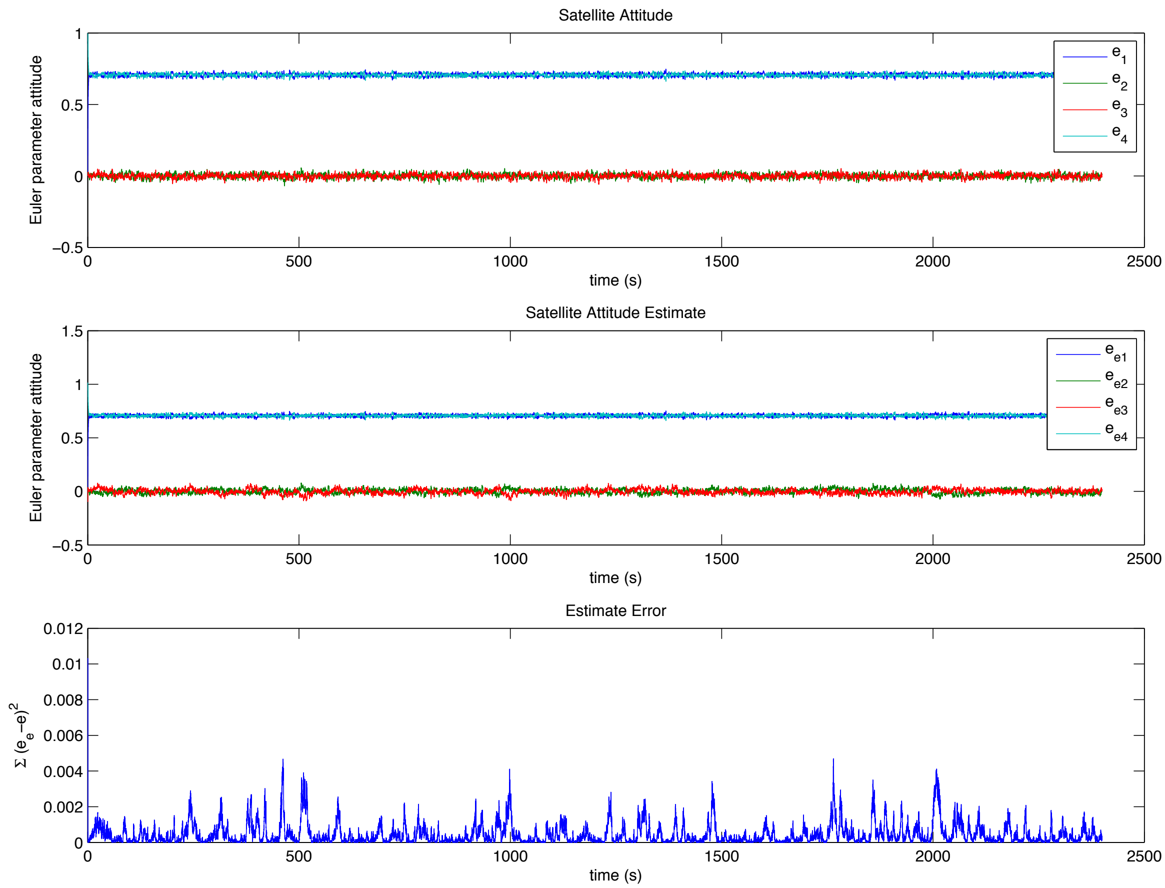

Figure 7.2: Attitude estimator simulation results using the dynamic and kinematic EKF

This simulation demonstrates the kinematic and dynamic EKF performance is significantly better than the performance of the attitude integrator alone. This method of presenting the errors, in the third plot, is unable to be directly translated to error in the estimated attitude but is able to give a general overview of the performance of the filter.

The main drawback for the kinematic and dynamic EKF is the size and complexity of the filter which will put a strain on the computing resources available on the Oculus. A simpler filter is preferable for the Oculus attitude estimator.

7.2 Kinematic Attitude Estimator

The second EKF attitude estimator was developed using only the kinematics equations for the satellite and the magnetic field reading outputs and as a result is much simple than the previous estimator. The kinematic equation for the satellite attitude is used to generate $\mathbf{\Gamma}$ and $\mathbf{\Phi}$ used in the filter. The gyro readings were used as inputs to the kinematic equation show in Eq. (7.20)

$$\dot{\vec{e}} = \frac{1}{2} \begin{bmatrix} e_4 & e_3 & -e_2 & -e_1 \\ -e_3 & e_4 & e_1 & -e_2 \\ e_2 & -e_1 & e_4 & -e_3 \\ e_1 & e_2 & e_3 & e_4 \end{bmatrix}^{-1} \begin{bmatrix} \omega_1 \\ \omega_2 \\ \omega_3 \\ -c(e_1^2 + e_2^2 + e_3^2 + e_4^2 - 1) \end{bmatrix} \tag{7.20}$$

As before Baumgarte stabilization was used in the kinematics. Process noise was added to $\vec{\omega}$ to simulate noise in the gyroscope readings and affects all states of the system.

The output equation, used to generate $\mathbf{H}$, is the same as the third part of the output equations from the kinematic and dynamic implementation and is shown in Eq. (7.21).

$$^{b}\vec{B} = \begin{bmatrix} e_4^2 + e_1^2 - e_2^2 - e_3^2 & 2(e_1 e_2 - e_4 e_3) & 2(e_1 e_2 + e_4 e_2) \\ 2(e_1 e_2 + e_4 e_3) & e_4^2 - e_1^2 + e_2^2 - e_3^2 & 2(e_2 e_3 - e_4 e_1) \\ 2(e_1 e_2 - e_4 e_2) & 2(e_2 e_3 + e_4 e_1) & e_4^2 - e_1^2 - e_2^2 + e_3^2 \end{bmatrix} {}^{r}\vec{B} \qquad (7.21)$$

Measurement noise was added to the body frame magnetic field value to simulate errors in the magnetometer readings. The states, measurements, and inputs are assigned to the variables used in the filter as follows:

$$\begin{bmatrix} x_1 \\ x_2 \\ x_3 \\ x_4 \end{bmatrix} = \begin{bmatrix} e_1 \\ e_2 \\ e_3 \\ e_4 \end{bmatrix} \quad \begin{bmatrix} y_1 \\ y_2 \\ y_3 \end{bmatrix} = \begin{bmatrix} {}^{b}B_1 \\ {}^{b}B_2 \\ {}^{b}B_3 \end{bmatrix} \quad \begin{bmatrix} u_1 \\ u_2 \\ u_3 \end{bmatrix} = \begin{bmatrix} \omega_1 \\ \omega_2 \\ \omega_3 \end{bmatrix} \qquad (7.22)$$

The kinematic only Kalman filter was simulated using the same values for $\vec{\omega}$ and ${}^{b}\vec{B}$ as were used in the kinematic and dynamic filter. The results of this simulation are shown in Figure (7.3).

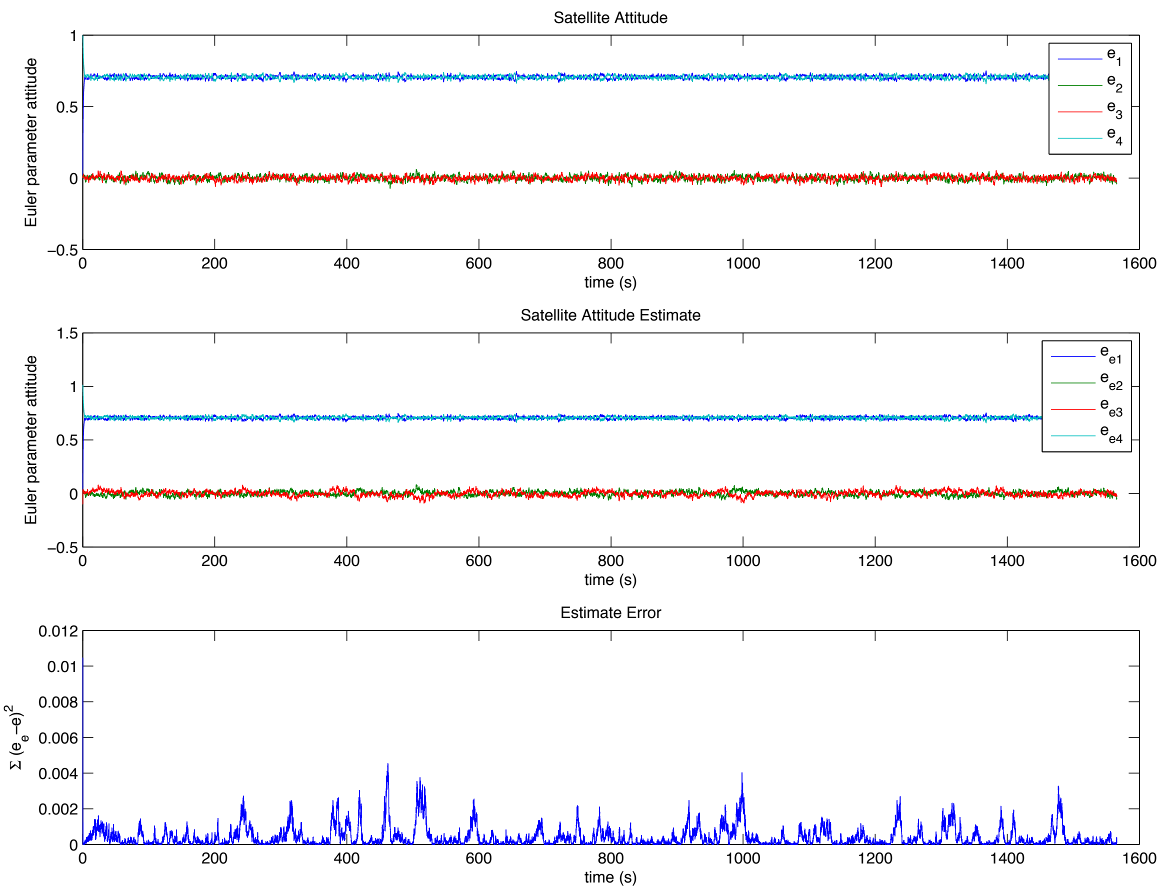

Figure 7.3: Attitude estimator simulation results using the kinematic EKF.

The kinematic only Kalman filter provides comparable performance to that of the kinematic and dynamic Kalman filter. The kinematic attitude estimator also is less complex than the previous Kalman filter allowing for less strain on the computing system on the Oculus. The kinematic only Kalman filter is expected to be used on the Oculus.

7.3 Magnetic Field Modeling Error

The error in the attitude estimate is caused by two main factors, the sensor noise, which is directly addressed by the Kalman filter designed in the previous sections, and the error in the magnetic field model. The error in the magnetic field is caused by an error in the calculated position of the satellite and the modeling error of the field itself.

The model of the magnetic field depends on two inputs, the time and the position of where the local magnetic field is to be modeled. The position of the Oculus while it is in orbit will be modeled using the Simplified General Perturbations Satellite Orbit Model 4 (SGP4) algorithm. The SGP4 algorithm propagates the position of satellite orbiting earth using a Two-Line Element (TLE) set for the initial condition. The TLE set does not come with an covariance estimate of the error, [6] but it is well known that the position of the satellite is in the kilometers range [19]. The error in position results in an error in the magnetic field model vector.

The second source for error in the magnetic field model is in the model itself. There are two magnetic field models which are commonly used, the International Geomagnetic Reference Field (IGRF) and the World Magnetic Model (WMM). Both of these models have comparable errors and the main difference is the source of the models. The accuracy of the either magnetic field model is dependent on the degree of the model. The attitude determination of the Oculus is dependent on the direction of the magnetic field vector. The angular error as a result of the IGRF model with a degree of seven at 300 km above the surface of the earth is expected is expected to be less than 0.3 degrees with a root mean square error of 0.1 degrees [20]. With increasing order the error in the field decreases. The WMM model used on the Oculus, can be computed up to a degree of 12 but a lower degree is desirable to reduce computation time.

These two errors in the magnetic field model are assessed through simulation. To simulate the error in the position of the satellite, ten kilometers was added in each direction to the position of the satellite represented in a three-dimensional cartesian coordinate system in the reference frame. Errors in the direction of the magnetic field vector were simulated by rotating the magnetic field 0.3 degrees about the z-axis, 0.3 degrees about the x-axis and again 0.3 degrees about the z-axis. The results of this simulation are show in Figure (7.4).

Comparing Figure (7.4) and Figure (7.3) reveals that the simulated sensor noise has a much greater effect on position of the satellite than the modeling error. To greater analyze the effect of the modeling error, the sensor noises were set to zero and the Kalman filter and its gains were unchanged. The results of this simulation are shown in Figure (7.5).

This simulation reveals the error caused by modeling the magnetic field is small in

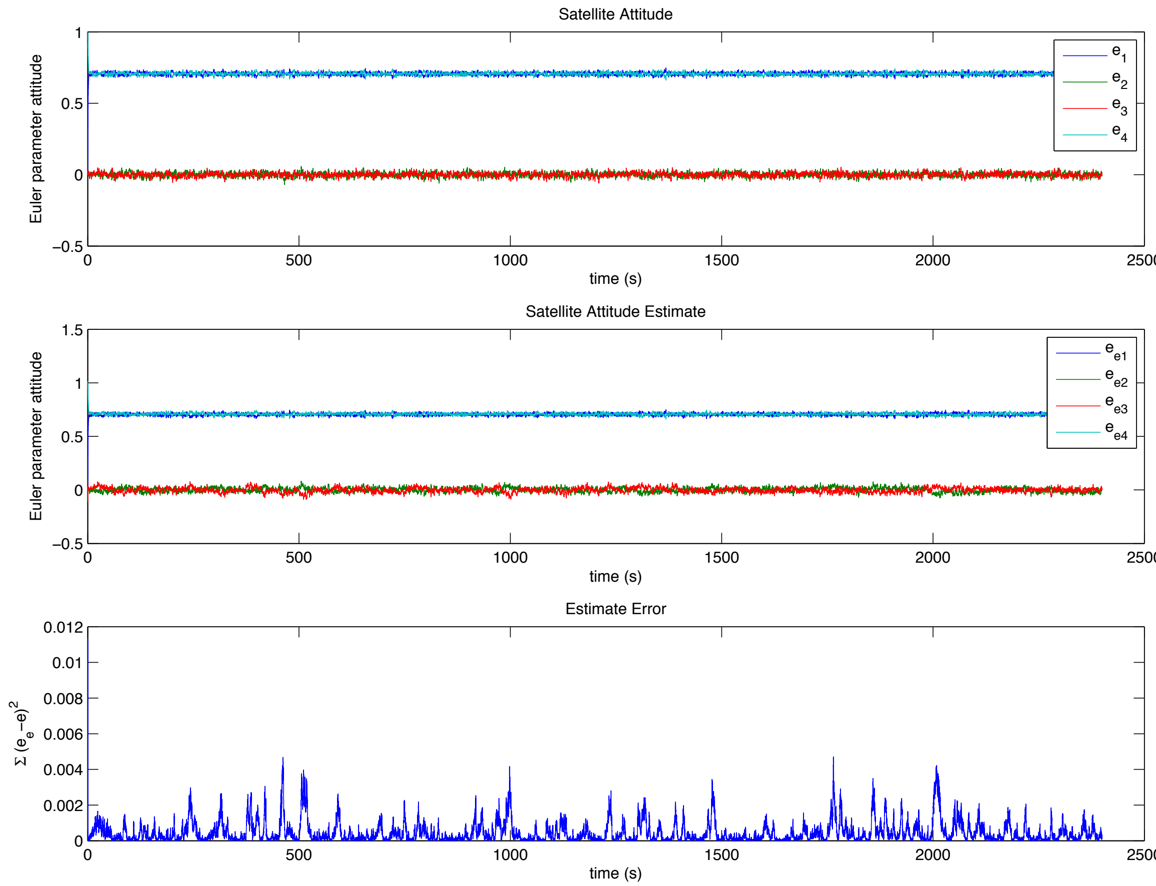

Figure 7.4: Attitude estimator simulation results using the kinematic EKF with measurement noise and model error.

comparison to the simulated sensor noise and can likely be ignored with respect to selecting the covariance matrices used in the Kalman Filter. Simulation with modeling error should be completed again once the noise characteristics of the sensors are determined and covariance matrices are selected.

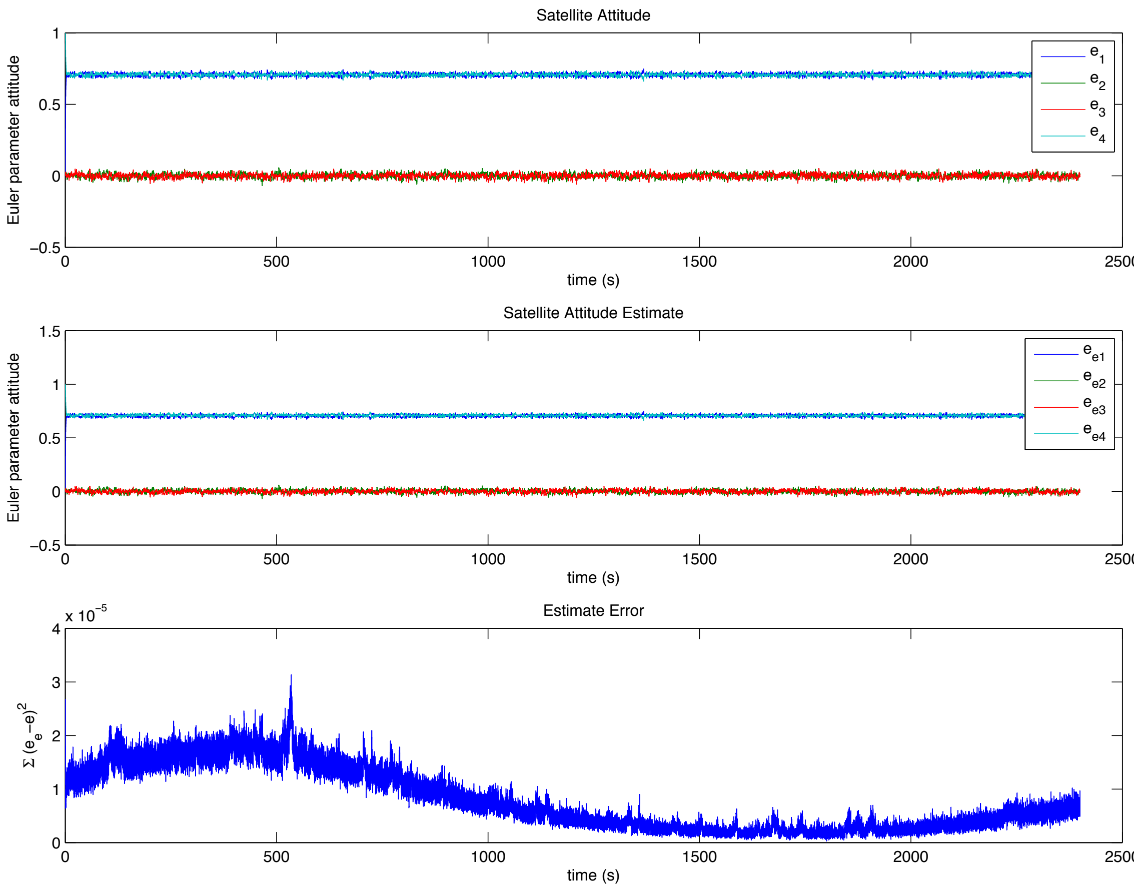

Figure 7.5: Attitude estimator simulation results using the kinematic EKF with model error and no measurement noise.

Chapter 8

Conclusions

The attitude control system for the Oculus was created to accomplish the space situational awareness technology demonstration mission. This system includes three main components, the reaction wheel controller, the magnetic torque rod controller, and the attitude estimator. These controllers were developed to meet the requirements stated in the introduction.

The first controller presented was the reaction wheel controller which addresses requirement 2, 3, 4, and 6. The primary purpose of this controller is precision attitude control for the visual servo task. Performance of the reaction wheel controller was demonstrated using simulation. Requirement 6 requires the satellite to be oriented to an arbitrary attitude such that the power generation from the solar cells is maximized.

Figure 5.1 and 5.2 demonstrate the ability to complete an inertial attitude change which is required to accomplish requirement 6. The simulation results demonstrate the system using the reaction wheel controller was type two and as a result capable of maintaining a slew rate bound only by hardware limitations and meeting requirement number 2. The reaction wheel control algorithm is capable of maintaining 0.15 degree pointing accuracy, satisfying requirement 3, for a wide range of maneuvers, as shown in Figure 5.1 through 5.4. The exception to this are maneuvers with large accelerations. Tracking the released imaging payload will not involve large angular accelerations. Finally, the reaction wheel controller is capable of tracking objects detected by the imaging apparatus, meeting requirement 4, as demonstrated by the simulated flyby and hardware in the loop simulation.

The magnetic torque rod controller was presented next. This controller's main purpose is maintaining the orientation of the satellite during non-precision operation and momentum management of the reaction wheels. The magnetic torque rod controller is used to meet requirement 1. Through simulation, it is demonstrated that the magnetic torque rod controller can detumble the satellite in less than one hour as shown in 6.1.

The final major component of the Oculus attitude determination and control system is the attitude estimator. Two attitude estimators based on the extended Kalman filter were developed. Both use Baumgarte stabilization to dynamically enforce the

Euler parameter constraint. The attitude estimator chosen for use on the Oculus is the extended Kalman filter based on the Euler parameter attitude kinematics. The attitude estimator is used on conjunction with the perviously discussed controllers to meet requirement 6 for orientating the satellite while not tracking or monitoring.

These three main components of the Oculus attitude control and determination system come together to accomplish the Oculus mission. The final step will be to integrate these components with the Oculus hardware and software including the imaging system. This task is being completed by members of the Oculus team in preparation for the selection of the launch opportunity satellite.

References

[1] Astolfi, A. and Lovera, M. (2002). Global spacecraft attitude control using magnetic actuators. *Proceedings of the 2002 American Control Conference*, 2:1331–1335.

[2] Baumgarte, J. (1972). Stabilization of constraints and integrals of motion in dynamic systems. *Computer Methods in Applied Mechanics and Engineering*, pages 1–16.

[3] Chang, C., Fu, L., Huang, C., and Yu, M. (2004). Sliding-mode tracking control of the stewart platform. *Control Conference, 2004, 5th Asian*, 1:562– 569.

[4] Chui, C. and G.Chen (1991). *Kalman Filtering with Real-Time Applications*. Springer-Verlag.

[5] Froelich, R. and Papapoff, H. (1959). Reaction wheel attitude control for space vehicles. *IRE Transactions on Automatic Control*, 4:139 – 149.

[6] Kelso, T. (2007). Validation of sgp4 and is-gps-200d against gps precision

ephemerides. In *17th AAS/AIAA Space Flight Mechanics Conference*. AAS Publications. AAS 07-127.

[7] Kulkarni, J. and Campbell, M. (2004). An approach to magnetic torque attitude control of satellites via 'h_∞' control for ltv systems. *43rd IEEE Converence on Decision and Control*, pages 273–277.

[8] Nicosia, S. and Tomei, P. (1992). Nonlinear observer and output feedback attitude control of spacecraft. *IEEE Transactions on Aerospace and Electronic Systems*, 28:970 – 977.

[9] Nudehi, S. S., Farooq, U., Alasty, A., and Issa, J. (2008). Satellite attitude control using three reaction wheels. *2008ÊAmericanÊControlÊConference*, pages 4850–4855.

[10] Parker, G. G. and Robinett, R. D. (1997). Least squares sliding mode control tracking of spacecraft large angle maneuvers. *Journal of the Astronautical Sciences*, 45(4):433–450.

[11] Peck, M. A. (2000). Attitude propagation with intermittent gyro measurements and single-vector observations. *AAS/AIAA Astrodynamics Specialist Conference*, pages 331–337.

[12] Psiaki, M. L. (2001). Magnetic torquer attitude control via asymptotic periodic linear quadratic regulation. *Journal of Guidance, Control, and Dynamics*, pages 386–394.

[13] Psiaki, M. L. and D'Andrea, R. (1999). Satellite attitude control using magnetic torquers, a periodic time varying control, final technical report for afosr grant f49620-99-1-0169. Technical report, Mechanical and Aerospace Engineering, Cornell University.

[14] Sadati, N., Meghdari, A., and Dadkhah Tehrani, N. (2002). Optimal tracking neuro-controller in satellite attitude control. *IEEE International Conference on Industrial Technology*, 1:54 – 59.

[15] Schaub, H. and Junkins, J. L. (2003). *Analytical Mechanics of Space Systems*. American Institute of Aeronautics and Astronautics, Inc., Reston, VA.

[16] Shoemaker, J. (2005). Space situational awareness and mission protection. `http://www.darpa.mil/DARPAtech2005/presentations/space_act/shoemaker.pdf` (accessed April 2008).

[17] Singh, S. N. (1986). Model reference adaptive attitude control of spacecraft using reaction wheels. *25th IEEE Conference on Decision and Control*, 25:1514–1519.

[18] Su, K., Ren, D., You, Z., and Zhou, Q. (2004). Application of mimu/magnetometer integrated system on the attitude determination of micro satellite. *Preceedings of the 2004 International Conference on Intelligent Mechatronics and Automation*, pages 579–583.

[19] Vallado, D. A., Crawford, P., Hujsak, R., and Kelso, T. S. (2006). Revisiting spacetrack report #3. Technical report. AIAA 2006-6753.

[20] Wertz, J. (2002). *Spacecraft Attitude Determination and Control*. Reidel Publishing Company.

[21] Wertz, J. R. and Larson, W. J. (1999). *Space Mission Analysis and Design*. Microcosm and Kluwer.